June 2016
Volume 122
Issue 1962
£5.60

www.electronicsworld.co.uk

Electronics WORLD

THE ESSENTIAL ELECTRONICS ENGINEERING MAGAZINE

SPECIAL REPORT
MEDICAL ELECTRONICS

- Lab-on-a-PCB
- Microfluidic chip
- Vital signs monitoring
- Power management

Electro Rent Europe proves to be the T&M business partner of choice

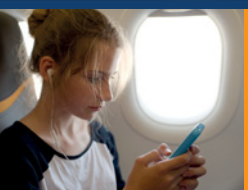

Technology
Mobile broadband is coming on planes next

Special Report
Medical device testing and standards

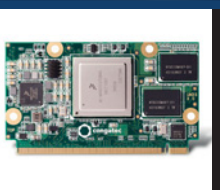

Products
Embedded computer modules, software and others

IMMEDIATE SHIPMENT FROM THE WORLD'S LARGEST SELECTION OF ELECTRONIC COMPONENTS™

1,300,000+ Products In Stock

FREE SHIPPING ON ORDERS OVER £50!*

Digi-Key® ELECTRONICS

0800 587 0991 • 0800 904 7786

DIGIKEY.CO.UK

4.8 MILLION PARTS ONLINE | 650+ INDUSTRY-LEADING SUPPLIERS | 100% AUTHORIZED DISTRIBUTOR

*A shipping charge of £12.00 will be billed on all orders of less than £50.00. All orders are shipped via UPS for delivery within 1-3 days (dependent on final destination). No handling fees. All prices are in British pound sterling and include duties. If excessive weight or unique circumstances require deviation from this charge, customers will be contacted prior to shipping order. Digi-Key is an authorized distributor for all supplier partners. New product added daily. © 2016 Digi-Key Electronics, 701 Brooks Ave. South, Thief River Falls, MN 56701, USA

ecia MEMBER ecsn member CEDA

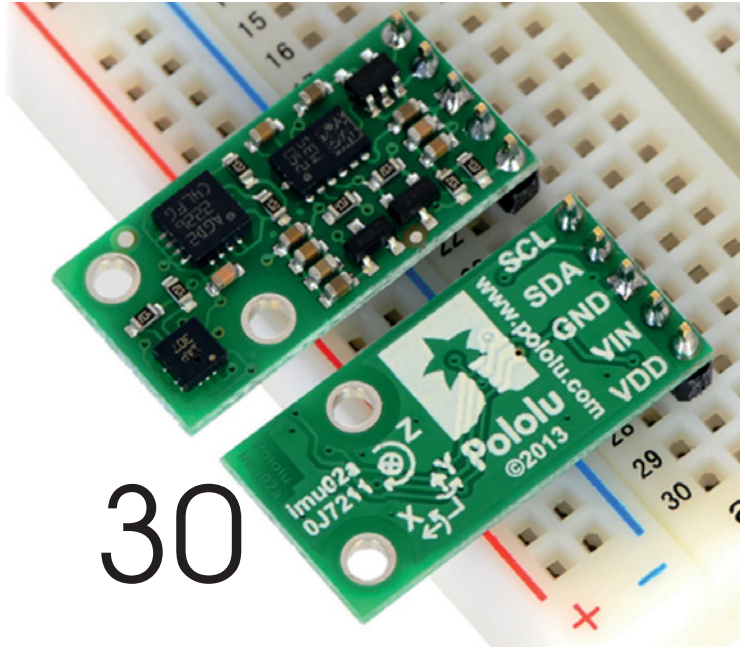

30

REGULARS

Cover supplied by
ELECTRO RENT EUROPE
More on pages 8-9

48

FEATURES

07

Disclaimer: We work hard to ensure that the information presented in Electronics World is accurate. However, the publisher will not take responsibility for any injury or loss of earnings that may result from applying information presented in the magazine. It is your responsibility to familiarise yourself with the laws relating to dealing with your customers and suppliers, and with safety practices relating to working with electrical/electronic circuitry – particularly as regards electric shock, fire hazards and explosions.

Improve 32-bit performance and connectivity with the PIC32MZ EF series

High speed and performance for high-bandwidth applications

A double-precision FPU, dedicated DSP pipeline and a high-performance 12-bit ADC allow Microchip's PIC32MZ EF series of 32-bit MCUs to improve code density, decrease latency and accelerate performance in process-intensive applications.

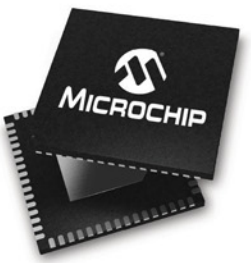

The 48 devices in the PIC32MZ EF family also offer up to 2 MB of dual-panel Flash and up to 512 KB RAM. A live-update capability allows the Flash to be updated whilst the CPU is in operation. The family also offers a rich peripheral set and more connectivity options than any other PIC32 MCU. These options include 10/100 Ethernet MAC, high-speed USB with PHY, high-speed SQI, and dual CAN ports.

In the LCCG configuration, the PIC32MZ EF family can drive WQVGA displays without the added cost of external graphics controllers. There is also support for high-throughput data encryption, decryption and authentication from the optional, full-featured hardware crypto engine with true random number generator.

microchip DIRECT
www.microchipdirect.com

MICROCHIP

www.microchip.com/get/eupic32mzef

The Microchip name and logo, MBLAB, and PIC are registered trademarks of Microchip Technology Incorporated in the U.S.A. and other countries. REAL ICE, and chipKIT are trademarks of Microchip Technology Inc. in the U.S.A. and other countries. All other trademarks mentioned herein are the property of their respective companies. © 2015 Microchip Technology Inc. All rights reserved. DS60001373A. MEC2041Eng09/15

DEVICE MANAGEMENT PROVES A BARRIER TO IOT AT SCALE

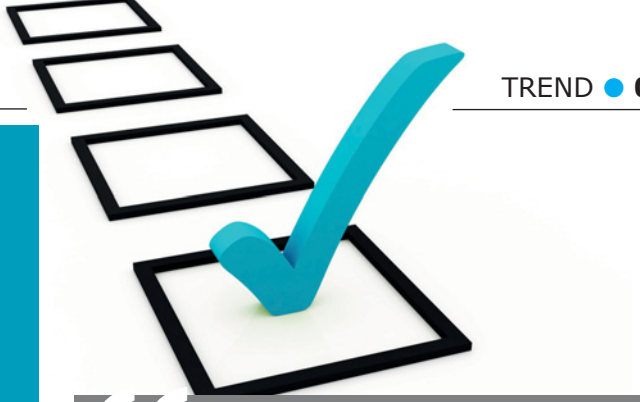

> Managing IoT devices is a complex hurdle within the IoT value chain

Managing Internet-connected devices in the millions or even thousands is seen as a major obstacle to the success of the Internet of Things (IoT), according to a recent survey conducted by IoT pioneer DevicePilot (previously 1248 Ltd). Some 50 companies participated in the survey, each planning to deploy IoT applications at scale across different industry sectors, including environmental and industrial monitoring, elderly care/ wellness, smart homes and cities, energy management, refrigeration, retail and public services.

The survey ranked "risk to growth" as the most worrying consequence of failing to manage devices, followed by "risk to revenue" and "risk to brand". This could help explain why some of the ambitious predictions for IoT devices have not been realized as yet.

Most survey respondents agreed that the biggest risk of not getting device management right is the risk to growth.

"Our business model is based on aggregating flexible energy demand from very large numbers of connected devices; having an accurate picture of how those devices are performing and simplifying how we connect and exchange information between multiple control systems and processes is a vital part of scaling our business and maximizing the value of the flexible energy demand we're tapping into," said Toby Coleman of demand response aggregator Open Energi.

Some 12% of the survey respondents had deployed a million or more devices in the field, 82% only 1,000 devices or less, and 18% describe their device management as "highly automated and slick".

"It is clear that most IoT companies are currently managing their connected products manually or by a mixture of manual and automatic processes," said Pilgrim Beart, CEO at DevicePilot. "But as projects move from pilot to deployment at scale, the time and operational cost of manually logging-in to each device to perform an upgrade or check if it is working becomes a major barrier. Automatic asset management, monitoring and lifetime support are essential for the long term success of the IoT."

"Managing IoT devices is a complex hurdle within the IoT value chain," added Zach Shelby, vice president of marketing, IoT business at ARM.

A remarkable 86% of survey respondents said that as far as managing devices is concerned, they're either already in trouble, or expect to be within 12 months.

"It sometimes surprises me how many device companies don't even know how many of their devices have been deployed, let alone how many are working. As the IoT matures, users' expectations of service quality are rapidly increasing and you really have to keep on top of this stuff. When it comes to the smart home, we expect all devices to be connected and providing useful information for owners and manufacturers on usage, diagnostics, need for refurbishment and replacement," said Cees Links CEO of GreenPeak Technologies.

However, respondents to the survey expect the number of connected devices to grow, with 70% expecting a market size of millions of devices and 20% predicting levels in the billions; 61% of companies anticipate 10x growth over the coming year.

"It's important to maintain our leadership in the smart refrigeration market – simply put this means connectivity which gives us the opportunity to collect sales data and insights remotely. At scale, the management of those connected devices has to be automatic to be cost-effective," said Colin Chapman, CTO of smart commercial refrigeration specialists Elstat.

Survey respondents said that for them the most common business model is a combination of upfront fee plus ongoing service fee.

"Connected devices are deployed into the physical world where lots of things can go wrong. For the IoT to work like the Web it needs an open ecosystem of interoperating, off-the-shelf products and services," said Beart.

The full survey report can be found on www.devicepilot.com. DevicePilot (formerly 1248 Ltd) developed the DevicePilot software for locating, monitoring and managing connected devices at scale

EDITOR:
Svetlana Josifovska
Tel: +44 (0)1732 883392
Email: svetlanaj@sjpbusinessmedia.com

SALES:
James Corner
Tel: +44 (0)20 7933 8985
Email: jamesc@electronicsworld.co.uk

Philip Woolley
Tel: +44 (0)20 7933 8989
Email: philipw@sjpbusinessmedia.com

DESIGN: Tania King

PUBLISHER: Wayne Darroch

ISSN: 1365-4675

PRINTER: Buxton Press Ltd

SUBSCRIPTIONS:
Subscription rates:
1 year: £65 (UK); £94 (worldwide)
Tel/Fax +44 (0)1635 879361/868594
Email: electronicsworld@circdata.com
www.electronicsworld.co.uk/subscribe

SJP business media

2nd Floor,
52-54 Gracechurch Street,
London, EC3V 0EH

Follow us on Twitter
@electrowo

Join us on LinkedIn

NEW! IP67 rated 12 to 36 watt encapsulated AC-DC power supplies for harsh environments!

Features

- 90-264VAC universal AC input
- Compact dimensions PS12MK 56x39x26mm, PS20MK 64x47x28mm, PS36MK 133x50x34mm
- Single DC outputs of 5, 9, 12, 15 or 24V
- IP67 fully encapsulated and waterproof
- Fixing holes for wall or chassis mounting
- Input and output connectors optional
  Comes with 400mm flying leads as standard
- No Load Power Consumption ≤0.3W max
- EN60950 & EN55022 safety & EMC standards (cTUVus approvals pending)
- Ideal for CCTV or LED applications
- Class II safety, no earth connection required
- CE marked and full safety approvals

Output Voltage & Current Ratings

MODEL	OUTPUT	MODEL	OUTPUT	MODEL	OUTPUT
PS12MK-05	5VDC 2A	PS20MK-05	5VDC 3A	PS36MK-05	5VDC 5A
PS12MK-09	9VDC 1.2A	PS20MK-09	9VDC 2A	PS36MK-09	9VDC 4A
PS12MK-12	12VDC 1.0A	PS20MK-12	12VDC 1.5A	PS36MK-12	12VDC 3A
PS12MK-15	15VDC 0.8A	PS20MK-15	15VDC 1.2A	PS36MK-15	15VDC 2.4A
PS12MK-24	24VDC 0.5A	PS20MK-24	24VDC 0.83A	PS36MK-24	24VDC 1.5A

POWER SOLVE

www.powersolve.co.uk
Email: sales@powersolve.co.uk Tel: 44-1635-521858

NXP AND PARTNERS DEMONSTRATE VEHICLE-TO-VEHICLE COMMUNICATION IN AUTONOMOUS TRUCKS

NXP Semiconductors and DAF Trucks have successfully demonstrated self-driving technologies in automated trucks. The demonstration was part of the European Truck Platooning Challenge, an event organized by the Dutch Ministry of Infrastructure and the Environment, designed to bring autonomous platooning (convoys) to public roads and prove its economic, traffic management and safety benefits. The Challenge also addresses the need for legislation and standardization of Intelligent Transportation Systems (ITS) across Europe.

"We're honoured to be part of the European Truck Platooning Challenge. NXP is helping to improve fuel efficiency, emissions, safety and traffic flow in the European Union, while avoiding accidents and saving lives," said Torsten Lehmann, senior vice president for Driver Assistance at NXP.

NXP, DAF, TNO and Ricardo are part of a consortium called EcoTwin that made this demonstration possible. At the heart of the EcoTwin setup is a sophisticated vehicle-to-vehicle (V2V) communication solution called RoadLINK developed by NXP. It uses the IEEE 802.11p wireless communication standard in combination with radar to enable trucks within a platoon to securely exchange information in real time and automatically brake and accelerate in response to the lead truck.

The high speed of communication and responsiveness allows extremely tight distances and synchronous driving between the trucks. For example, the planned distance between the vehicles was determined to be 0.5 seconds, which when traveling at 50mph translates to a distance of only 10 metres. The responsiveness of the trailing trucks within the platoon is estimated to be 25 times faster than the average reaction time of one second for a human – saving critical time in case of emergency braking.

Autonomous truck convoys will soon be on the public roads

The RoadLINK communication system is built into the truck mirrors. The system has four secure channels and allows real-time video and bi-directional audio communication between vehicles. It enables the trucks to automatically exchange information on speed, position and direction between them or other RoadLINK-enabled vehicles and infrastructure. Communication could further consist of traffic management data or hazards such as localized speed limits, traffic signalling, roadworks warnings, trecherous location conditions and more.

"This is definitely not a process that will be complete before 2020. There is still a great deal that has to be sorted out in terms of legislation, liability and acceptance," said Ron Borsboom, member of DAF Trucks's Board of Management.

NXP is working with car OEMs including Siemens, Harman, Delphi and Cohda Wireless to implement its technologies. Its RoadLINK is already scheduled for integration in different car models starting this year as part of the Delphi V2X platform.

LOW-COST MOBILE BROADBAND WILL SOON BE AVAILABLE TO AIRLINE PASSENGERS

Professor Yang Hao from Queen Mary University of London has been working on a new satellite antenna that will enable broadband services to passengers on planes. Today, air passengers have to switch off their mobile phones or use 'flight mode', and pay additional charges to access data on their devices.

"Our goal is to make low-cost smart antenna systems an engineering reality that can be enjoyed by everyone, from professionals in satellite communications to air passengers who want to stay connected on their mobile phone or devices," said Professor Hao.

He predicts widespread use of this technology within a short time and is working with partners to collectively redefine satellite transmission theory with his cutting-edge antenna design to enable a seamless broadband experience from land to air, at no additional cost to users.

Switchting off cellphones on planes will soon be a thing of the past

HOW TO RECRUIT THE BEST ENGINEERS

How having the right test equipment at an affordable cost can help small and medium sized companies recruit the best young engineers

By André Vandenberk, Sales Operations Manager, Electro Rent EMEA www.electrorent.co.uk

There is a shortage of good engineers in EMEA, and the young engineers coming out of colleges and universities know this and gravitate towards the big name companies. Smaller companies, even though they may be working on large projects, often find it hard to attract the best people.

I came across this problem when dealing with a medium-sized engineering company in Europe. The firm provides small satellites, space mechanisms and structures, and instruments and facilities for micro gravity research on manned and unmanned space missions.

With many young engineers dreaming about working on space projects, I assumed that the company would have no problem at all attracting engineers. But this was not the case. Because it was not widely known, it found itself fighting over the top engineers with larger organisations.

As such, the bosses at the company started looking for ways to make their workplace a more attractive prospect for a new engineer. The budget was limited so they could not throw vast amounts of money at the problem, either in large salaries or expensive equipment that would tempt new recruits. Plus, the company only took on a new graduate now and again, a factor that made it even more important to find the right person.

Test equipment

However, one difficulty many young engineers face when they join a company is a shortage of dedicated test equipment. Typically, they have to share test equipment with the more experienced engineers or even have to book time on the equipment. Buying them their own equipment is often too expensive. A new 26GHz high-end spectrum analyser, for example, can easily cost in the region of £45,000, and having one of those per person is a large chunk of the budget.

The space company had a policy of its capital expenditure budget being allocated per project per year and, though junior engineers were contracted to work on these projects, they found it difficult to defend such large investments for a product the engineer was not going to be using all the time.

This is not uncommon. Small engineering companies come up against this regularly where their new engineers are not given access to a lot of test equipment. A spectrum analyser each almost never happens.

Yet for the engineers it can be more fun in their jobs if they can test projects as they go along. They are also more efficient when they are trying out new ideas. They have not got the experience to work an idea through and do not

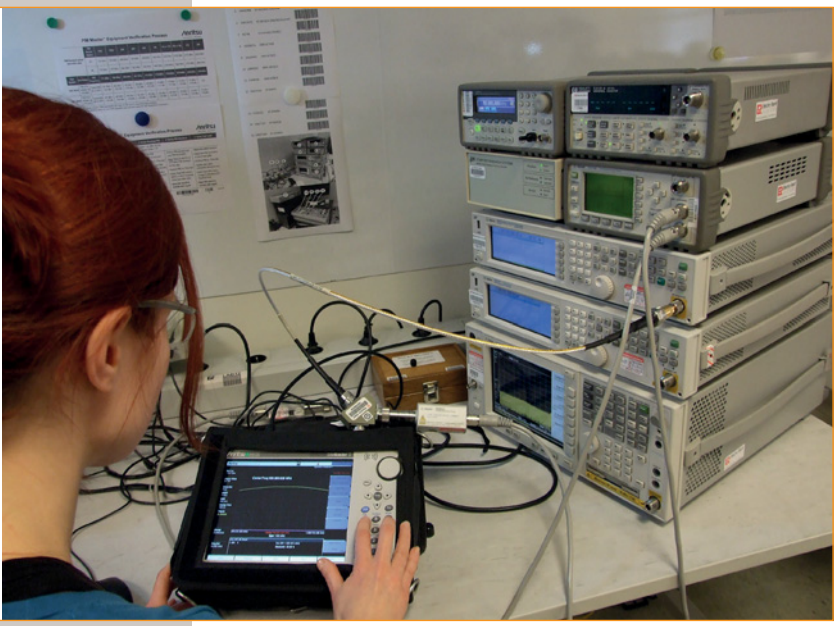

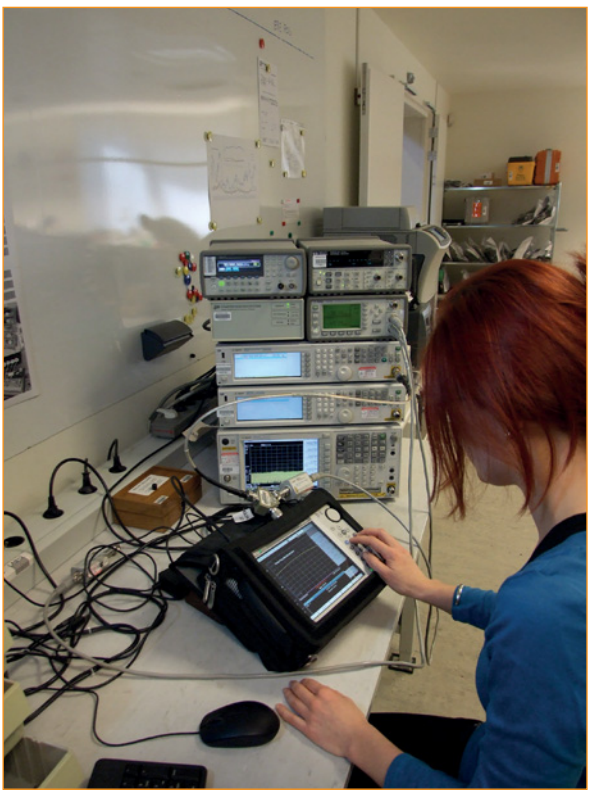

want to have to wait until test equipment comes free to test their ideas. But if they could have easy access to the test equipment, it would boost their efficiency on the project and take away a lot of theoretical mistakes.

For example, with the test equipment on hand, they can experiment. On a mathematical model, they can put in ridiculous values to see what would happen, but they cannot do that in the real world. Having the test equipment handy lets them carry out this kind of experimentation as they go along, thus boosting their productivity. They also learn and improve at a faster rate if they have the means to check what they are doing.

Having their own equipment also helps overcome an understandable shyness about having to keep asking more experienced colleagues to borrow their equipment.

Alternative

All this is why having a dedicated test instrument for a young engineer can be a good investment. But for smaller enterprises, that £45,000 for a spectrum analyser is a lot of money. However, the young engineer is often just checking the basics for which he or she does not require a brand-new top end analyser. This is especially true when working in the RF domain where the latest equipment offers few advantages, yet the basics still have to be learned.

The space company I mentioned took the decision to look at the used equipment market and approached Electro Rent Europe. Here, the bosses found that they could spend £13,970 on a 26GHz spectrum analyser. Using the Flex Term service, this investment could be spread over two years, resulting at just £582 per month, well within the budget for the project.

The company tried this with a new engineer a few years ago and was so impressed that this has now become standard policy whenever an engineer is hired. This does not lead to them having more applicants when they enter a recruiting round but it does make it easier to convince the applicants they do get that the company is a worthwhile employer.

Conclusion

Attracting the best engineers during a shortage can be difficult for small and medium sized companies. But rather than throwing a lot of money at the problem, it is better to give them access to equipment that makes their job more enjoyable and productive. And by going to the used equipment market and spreading the payments, this can be far less expensive than many imagine. Good test equipment can be made available at just a small outlay per month.

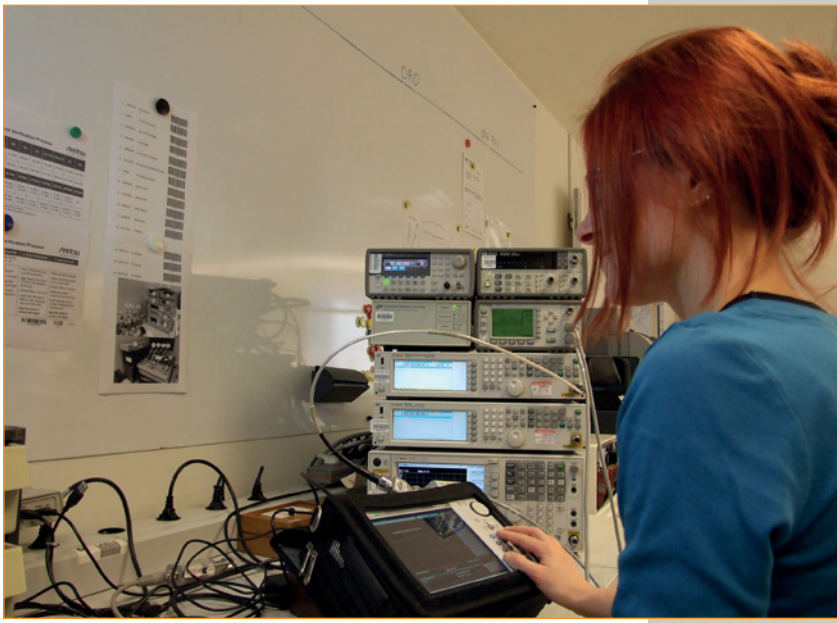

As the small European space company has found, for a negligible impact on budget, it can now compete with some of the larger players when it comes to recruiting the latest engineers. Once recruited, the young engineers become more productive and learn their trade much more quickly. And these factors can be critical for any small and medium enterprise for without the new blood with their new ideas the way forward can be tricky to say the least.

A BLE Servo

BY **LUCIO DI JASIO**, MCU8 BUSINESS DEVELOPMENT MANAGER AT MICROCHIP TECHNOLOGY

Servo motors are a fun and inexpensive way to animate objects. One example is the 'Cookie Monster' project featured in the last issue, where I explained how to control servos using simple PWM peripherals and how to build PWMs by assembling a few configurable blocks, taking advantage of the core independent peripherals (CIPs) and the flexible design of modern 8-bit microcontrollers. This month we will add wireless remote control to the servo application using the latest Bluetooth Low Energy (BLE) technology. We will also use the MPLAB Xpress cloud toolchain to avoid lengthy installations, the MPLAB Xpress evaluation board for rapid prototyping and MPLAB Code Configurator (MCC) for a quick configuration of all required microcontroller peripherals.

BLE

Bluetooth was originally developed over twenty years ago as a short-link radio (that was its actual name!) to solve common cabling problems in personal computers and consumer devices. It is based on a spread-spectrum frequency-hopping technology and uses the 2.4GHz ISM band.

Early designs mostly concerned audio connectivity (wireless headsets) but its popularity grew rapidly that with the release of the 4.0 (and later) specifications and the introduction of the new low energy technology (or BLE for short) it's become a symbol of sorts for the "Internet of Things" today.

Despite the common root name, Bluetooth Classic and the newer BLE are substantially different. Although radio modules supporting both technologies exist (they are now sold as "Bluetooth Ready"), here we will focus only on the newer BLE variant.

BLE uses a packet-based protocol to rapidly transfer data between clients and servers with maximum energy efficiency. A server is typically represented by a sensor-based device. BLE uses so-called Generic Attribute Profile (or GATT) as application interface to facilitate data exchanges between servers and clients. In the GATT lingo, a server will make a number of characteristics (data) available to its clients, and a number of these are grouped into a "service". Both, services and characteristics, are uniquely identified by 128-bit numbers, called UUIDs.

The most common types of services and their characteristics have been pre-codified in the BLE specifications to provide ready-to-use profiles for various sensor uses, such as blood glucose meters, heart rate monitors, thermometers and so on. For convenience, such common services and characteristics can be identified with short 16- and 32-bit UUIDs.

For example, a battery service will be accessible with the (short) UUID: 0x180F and will include the characteristic

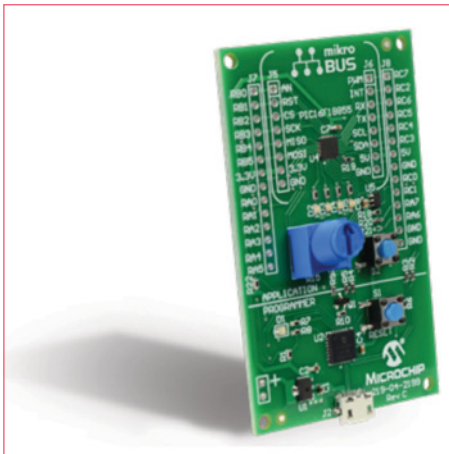

Figure 1: MPLAB Xpress evaluation board

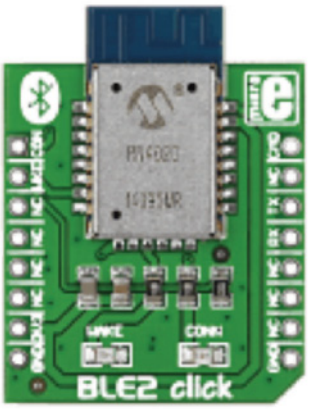

Figure 2: BLE2 click board

battery level with the (short) UUID: 0x2A19.

If you are familiar with the Bluetooth (Classic) profile definitions, you will soon realize that the approach is very different here. For example, there is no standard Serial Port Profile (SPP) to provide a direct emulation of a serial port over BLE. Instead, re-creating an SPP-like service with BLE is just a matter of defining a pair of characteristics (transmit and receive buffers) and offering the service UUID as a de facto standard. This is exactly what Microchip has done by defining what is now called MLPD, an option readily available in all its BLE modules at the closure of a contact.

BLE2 Click

A fast and easy way to experiment with BLE is to use the MPLAB Xpress evaluation board (or an MPLAB Curiosity board) and to connect an inexpensive BLE2 Click module via the mikroBUS connector with a click (pun intended).

This little board features an RN4020 BLE radio modem that encapsulates all the complexity of the Bluetooth stack in a few simple ASCII commands over a serial port. In fact, half-a-dozen (single character) commands will cover all the needs of an average embedded application. The user manual goes through a detailed description of each command and its parameters but, as often is the case, I found that the best way to learn how BLE works is to play with it!

The BLE Express

It is easy to turn the MPLAB Xpress evaluation board into a BLE terminal. Thanks to the core-independent features of the PIC16F18855 we can directly connect the Xpress evaluation board's USB serial port to the BLE module serial port pins on the mikroBUS connector using only two of the CLCs (configurable logic cells) and the PPS (peripheral pin select).

Creating a new project using the MPLAB Xpress IDE takes seconds and is as easy as opening a browser, entering the MPLAB Xpress URL https://mplabxpress.microchipcom and logging into your own MyMicrochip account.

Using MPLAB Code Configurator we can establish all the connections as shown in Figure 3; we will connect:

- Pin Click_RX (RC6) as the CLCIN0 input
- Pin USB_TX (RC0) as the output of CLC1
- Pin USB_RX (RC1) as the CLCIN1 input
- Pin Click_TX (RC5) as the output of CLC2

Both CLCs will be used as passthroughs, so an AND/OR configuration will suffice where only the top gate will be connected to one of the CLCINx pins (CLCIN0 for CLC1 and CLCIN1 for CLC2) and the second gate output will be simply inverted to provide a constant high level as shown in Figure 4.

To activate the RN4020 module we will also need to control the RST pin (RB1), initializing it as an output (starting high).

Once the configuration is "generated", the project can be

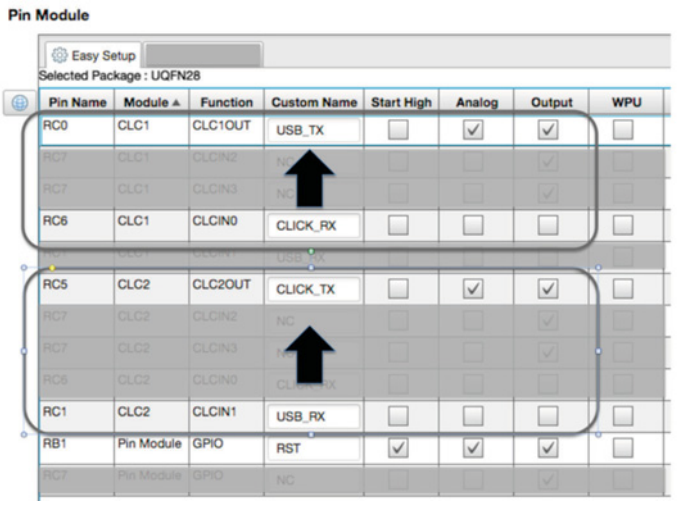

Figure 3: BLE Express connections

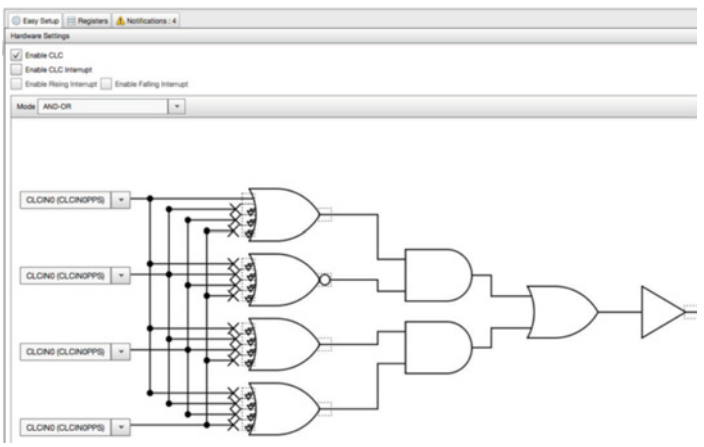

Figure 4: CLC passthrough configuration

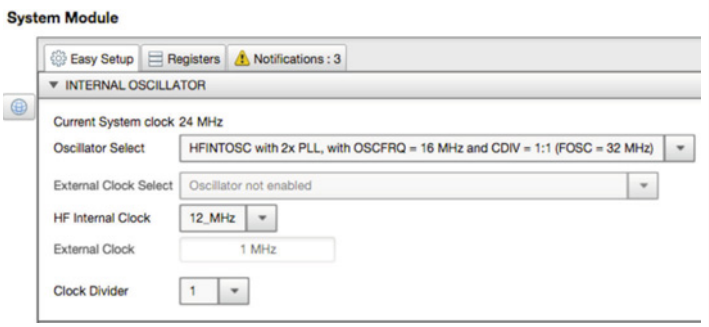

Figure 5: System Module configuration

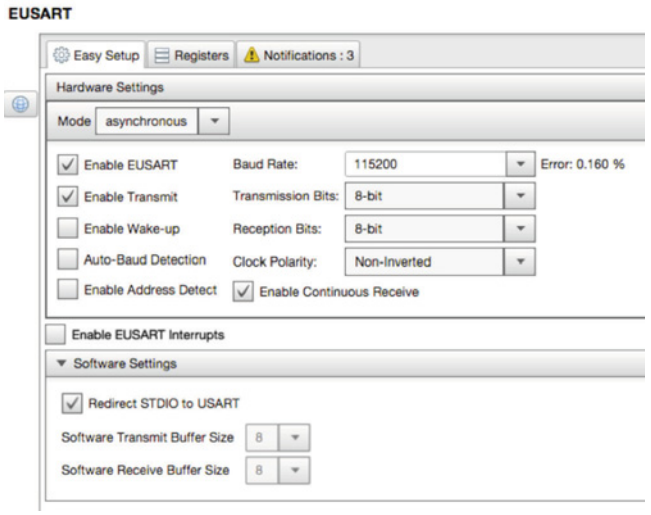

Figure 6: USART configuration

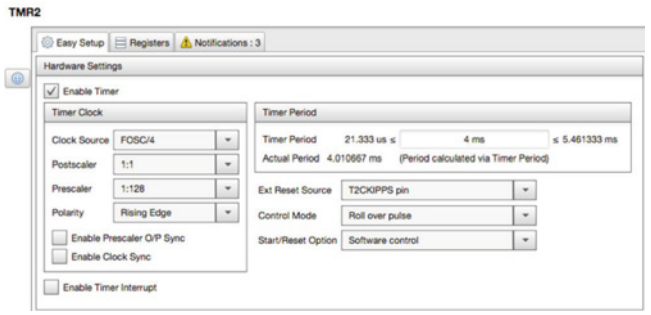

Figure 7: Timer2 configuration

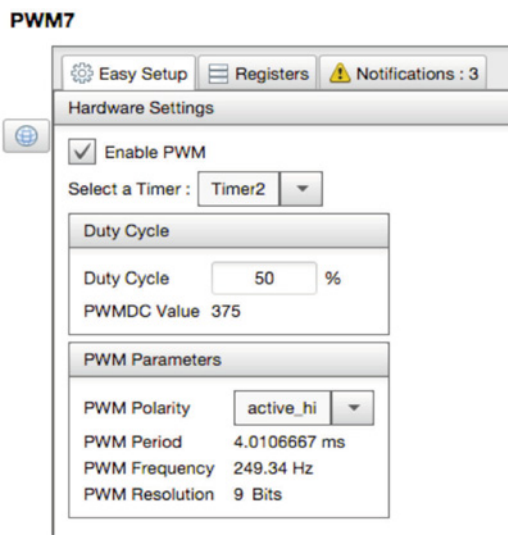

Figure 8: PWM8 configuration

immediately built and programmed to the MPLAB Xpress evaluation board, before physically connecting the BLE2 click board. If all goes well, you will be greeted by a blue LED light, indicating the module is powered and enabled.

Launch your favourite terminal program and set it to the default communication baud-rate, 115,200 (8-bit, no parity). You can now type commands directly to the terminal and see the BLE module repond. For example, typing a capital 'D' character followed by Enter will produce a short summary of the module status, likely to resemble the following:

```
BTA=001EC01CFCD4
Name=RN4020_FCD4
Role=Peripheral
Connected=no
Bonded=no
Server Service=00000001
```

Welcome on board the BLE Express!

Custom Service

Typing commands directly from the terminal we get to experiment interactively with the RN4020 command set. For example, we can learn how to set up a custom service – say, to drive a servo, or how to configure its characteristics – say, the servo position or PWM duty cycle.

So we discover that:

- to ensure that we start from a clean slate, we can use the "SF,1" command to restore the "factory settings".
- setting a "private" service can be accomplished by sending the "SS" command and passing the 32-bit mask 0x00000001.
- making the module act automatically as a server and start advertising its service at power-up is accomplished by the command "SR" and passing the 32-bit mask 0x20000000.
- the actual service UUID can be assigned with the "PS" command followed by a long string of 16 hexadecimal characters.
- the actual characteristic UUID can be assigned with the "PC" command, followed by a similarly long hexadecimal string, to specify if the data is input or output (and whether it will provide immediate notifications when changed) and, finally, a byte count.
- for a configuration to take, all such commands must eventually be terminated by a reboot of the module using the "R" command.

A BLE Servo Application

With the MPLAB Xpress cloud IDE, at this point it is easy to create a new application for the evaluation board where, this time, we will connect the PIC16F18855 serial port (EUSART) to the BLE module (TX/RX pins of the mikroBUS). We will also configure a PWM peripheral to drive a small servo motor and connect its output to a pin that is conveniently close to GND and to the 5V supply, such as RC3. This is not used by the BLE2

click and is available on the the evaluation board's outer ring of contacts (connector J8).

Thanks to MPLAB Code Configurator, this will take only a few more mouse clicks. Here's the procedure, step by step:

- Select the System Module configuration.
  Select HFINTOSC with 2x PLL configuration: 12MHz, internal clock. This will produce a 24MHz clock that will provide the most accurate approximation of the baud rate required by the EUSART; see Figure 5.
- Add the EUSART to the project resources.
  Configure it to operate at 115,200 baud and enable "Redirect STDIO to UART" to be able to use standard C I/O library to access the serial port, including printf(), puts(), putch() and getch(); see Figure 6.
- Add Timer2 to the project resources.
  Configure it to produce a 4ms time-base as shown in Figure 7.
- Add the PWM7 module to the project resources.
  Configure it to use Timer2 as shown in Figure 8.
- Select the Pin Manager configuration table and assign input/output functions to the appropriate pins as shown in Figure 9.

With a click of the "Generate" button, the MPLAB Code Configurator will produce the configuration files and place them in project sources. We are now ready to start focusing on the core of the application.

In 10 Lines Of Code

Listing 1 shows an example of an initialization function, to be delivered by the microcontroller at power-up. Actually, since the RN4020 module featured on the BLE2 click uses non-volatile memory to store its configurations, there is no need to repeat the process at each power-up, but perhaps only upon the very first time the application is launched or when the user so wishes, pressing a button. We can add this function to the main.c file that MCC generated from the standard template.

```
void BLE_Initialize( void)
{
 while(INPUT_PENDING) getch(); // flush input buffer
 sendCmd("SF,1"); // reset factory setting
 sendCmd("SS,00000001"); // private service
 sendCmd("SR,20000000"); // auto-advertise
 sendCmd("PZ"); // clear all prev. services
 // define a new service
 sendCmd("PS,00035b0358e607dd021a08123a000300");
 // define a new writable, notified characteristic
 sendCmd("PC,00035b0358e607dd021a08123a000301,18,01");
 // reboot to make changes effective
 sendCmd("R,1");
 __delay_ms(500);
}
```

Listing 1: Initializing the BLE module

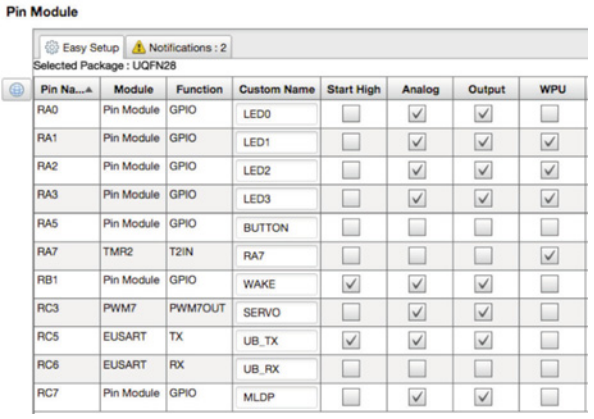

Figure 9: Pin Module configuration

Figure 10: SmartData available peripherals list

Figure 11: SmartData MLDP Send dialogue

The BLE_Initialize() function relies on its sendCmd() function to send a (constant) configuration string and then awaits the module's reply.

Should there be no reply within a given amount of time, or should the module simply reply with an error, the sendCmd() function would have the option to alert the user or simply keep re-trying, as desired. The actual implementation of this function will be omitted here for simplicity.

Note also how the UUID strings used in the BLE_Initialize() function are those used by the MLDP serial interface profile emulation service mentioned in the introduction. Be sure to type them in correctly.

We can now modify the main() function to incorporate the new initialization sequence at the push of a (user) button, and to await notifications on the receive characteristic.

```
void main(void)
{
 SYSTEM_Initialize();

 while (1)
 {
 if (BUTTON_PORT == 0){ // button forces the BLE
config
 BLE_Initialize();
 while(BUTTON_PORT == 0); // ensure button is
released
 }

 if (INPUT_PENDING) {
 char *msg = getLine(); // get the notification
 if (*msg == 'W') { // it is a write notification
 // 0123456789A
 // WV,00hh,XX.
 uint16_t servo = xtoi(&msg[8]); // value (0-180)

 // convert to duty cycle
 uint16_t duty = 102 + (servo*37)/18;

 // update servo position and display (lsb)
 PWM7_LoadDutyValue(duty);
 LATA = servo;
 }
 }
 }
}
```

Listing 2: Initializing the BLE module

Every time a new value is written to the receive characteristic, the BLE2 module will send a string of the following format:
WV,00hh,XX

where **00hh** is the handle of the characteristic being updated and **XX** is the (hexadecimal representation) of the new value.

Since we have defined a single characteristic (servo position), we won't bother to match the handle passed in the notification message. Instead, we will simply extract the new value, convert it to an integer and format it to a valid duty cycle range, ready to drive the servo.

In other words, the servo position values (0-255) need to be scaled and offset appropriately to produce output pulses between 0.5ms and 2.5ms in duration.

Note that for debugging purposes we are also going to copy the servo value to the four-LED string on the evaluation board.

Since we used the MLDP service UUID, we can now test the application using SmartData, one of the convenient apps provided by Microchip (for iPhone and Android) that support the MLDP serial emulation.

Figure 12: BLE Servo App screenshot

Upon launch, SmartData will present a list of devices that are actively offering an MLDP service (such as our BLE2 click application). Selecting a device from the list (RN4020_FCD4 in this case, the last four digits being part of the unique BLE module serial number), Smart Data attempts to connect and if successful will show a dialogue window where we can enter data to be sent.

Type a single character (our application is expecting a single byte) and press the send button. If you have a servo connected, it will promptly swing to a position that is proportional to the ASCII value of the sent character. The string of LEDs will also reflect its 4 LSB.

Beyond SmartData, the ultimate experience can only be provided by writing a native custom application for Android and/or iPhone. Figure 12 shows a screenshot of one such application I created to control the servo using a slider widget (shaped as the MPLAB Xpress logo/badge). ●

OLSON®

UK's No.1 IEC Connection

For further details of our extensive product range please call or email us on:

T +44 (0)20 8905 7273 E sales@olson.co.uk www.olson.co.uk

QMS ISO 9001 REGISTERED FIRM GB 1907

Manufactured in the UK

Gesture-controlled wireless automation

BY **DR DOGAN IBRAHIM**, PROFESSOR AT THE NEAR EAST UNIVERSITY, CYPRUS

As technology advances, the traditional interaction techniques designed to access computers and other devices face great challenges. Future human-computer interaction is being replaced by natural and multimodal techniques.

Gesture control is a strong candidate for future human-computer interaction; people use gestures in their everyday life. It is very common for people to move their hands whilst giving directions or when describing something to other people.

In general terms, gesture control is the process of natural interaction with a computer (or other device) without touching it, and by movement of fingers, head, eyes or even foot.

Gesture control is a way for computers to understand human body language, thus building a stronger bridge between the two. Most graphical information processed by computers is nowadays in 3D (especially in games); but, it is difficult and cumbersome to provide such complex input using traditional 2D input devices.

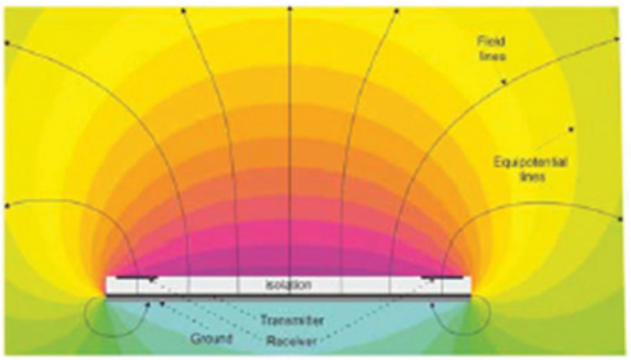

Figure 1: Equipotential lines of an undistorted e-field
[Credit: Microchip]

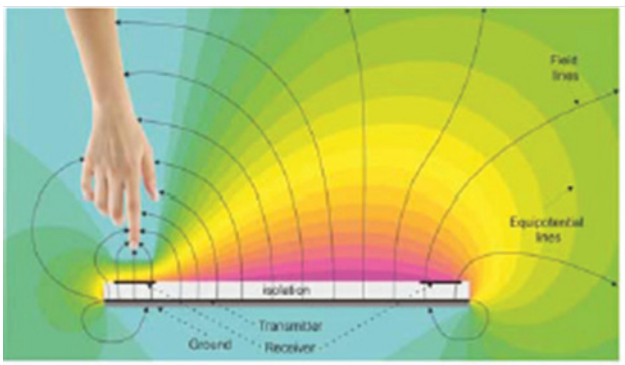

Figure 2: Equipotential lines of a distorted e-field
[Credit: Microchip]

Gesture-based hand control can be used in such circumstances to provide the required 3D input to a computer. One possible use could be whilst cooking for example – when following a recipe on a computer but the hands might be too dirty to turn the page. This could easily be achieved in gesture control by moving a finger over a sensor panel.

Another example is turning down the TV volume very quickly. Instead of searching for the remote control, gesture control can control the volume by using simple hand movements.

Although there are alternative solutions to touchless control, such as speech recognition, they do have limitations, especially when the environment is noisy.

Freehand gesture is the most common interpretation when people think about gestures. Here, gestures are defined completely by the movement of a user's fingers or hand, although some researchers have studied gesture control by the movement of the arm, foot or eyes.

Gesture-based applications can be used in many different fields, including entertainment, home appliance control, home and office comfort, elderly and disabled care, telecare and so on.

Although gesture-based interaction seems to be attractive and much research has gone into this field, there are still problems to address, such as standards and simplifying the systems.

Gesture States

User interface with gesture-based systems is in four stages: wait, collect, terminate and execute. The wait state is the dormant state where the system waits for the user to initiate a gesture command. When the user begins a gesture command the collect state is entered and the system captures gestural data from the input hardware. The terminate state is the recognition of the end of gesture. This usually occurs in one of three ways:

- End of the gesture is indicated by an external action, such as releasing a button.
- End of the gesture is indicated by an internal timeout.
- The system terminates the gesture because it has seen enough to recognise the command.

The execute state is when the required action is performed by the system.

Figure 3: Example gesture controller system

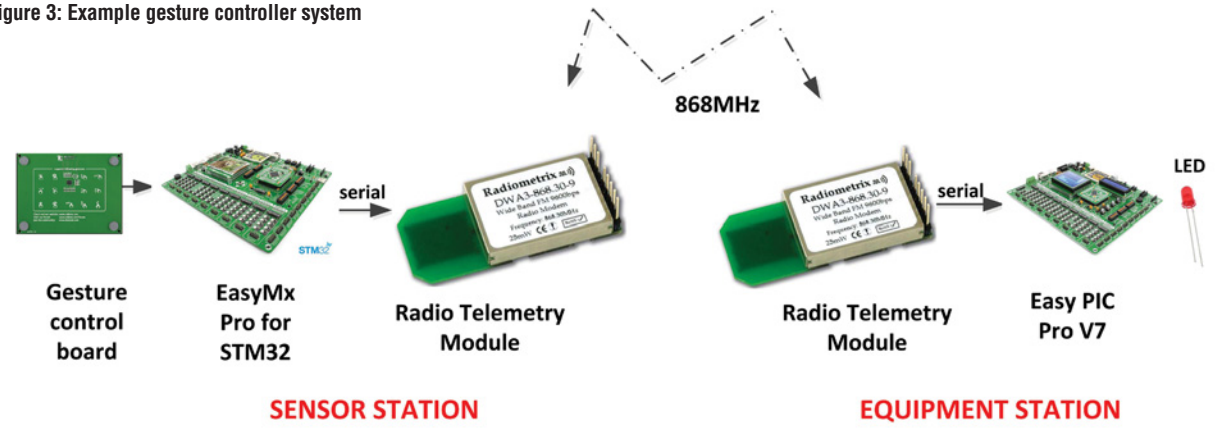

Gesture Detection

Gesture movements can be detected either visually or by electric field techniques. In a visual-based system, a camera captures movements of the hand or foot. These pictures are processed by a computer and translated into simple commands.

A visual system is easy to interact with, but may fail to recognise a gesture because of the complexity of the required image processing. An alternative is to use a specially built electronic wand whose movements can be sensed. A passive wand is also used in some applications with the movements tracked in space through computer vision techniques. In a similar manner, wired gloves, or "intelligent gloves", are also used as sensors, with the finger movements detected by the gloves and appropriate commands sent to a computer through the glove's electronics.

In an electric field system, a specially coated tablet is used which detects and processes the movement of fingers over the tablet.

Electric-Field-Based Gesture Sensor

Electric fields are generated by electric charges and propagate three-dimensionally around a surface as shown in Figure 1. When a person's finger or hand is in the electric field, it becomes distorted as shown in Figure 2, and the field lines are drawn to the hand as a result of the conductivity of the human body. The gesture control chip uses multiple electrodes to detect the electric field variations at different places to measure the origin of the electric field distortion from the received signals. This information is used by the gesture control chip to calculate the position and movement of the hand.

Example System

The design of a gesture-controlled automation system using an electric-field-based sensor is given here. The sketch of the designed system is shown in Figure 3. In most gesture control systems there are two parts: sensor station and equipment station. The gesture sensor is located at the sensor station

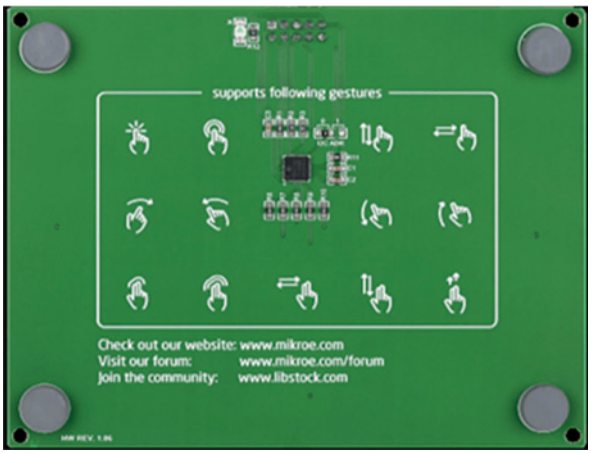

Figure 4: Gesture control board

where the finger or hand movements are detected, converted into commands and then transmitted to the equipment station, where the actual equipment is controlled.

In this example, the gesture controller system used at the sensor station is based on Microchip's MGC3X30 3D gesture recognition and motion tracking control chip. A gesture control board is available with this chip at the heart of the board (Figure 4). The movement detection range of the board is 16cm, and the board responds to various finger and hand movements, such as touch gestures, left to right or right to left hand or finger movements,

Figure 5: DWA3 Transceiver module

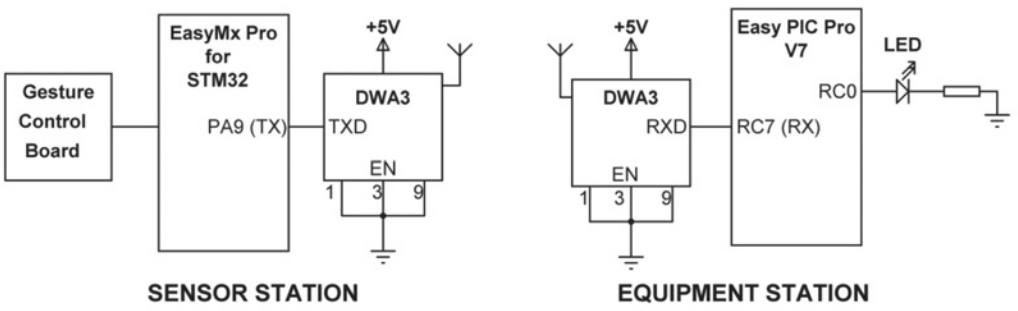

Figure 6: Block diagram of the example system

top to bottom or bottom to top hand or finger movements, flick and circle gestures and so on.

The gesture controller board is connected to the mikroBUS socket 1 of the development board through an adapter. The finger and hand movements are converted into simple commands by the microcontroller and are transmitted to the equipment station using an RF transmitter modem. In this design, a DWA3 UHF transceiver module from Radiometrix is used, which is a single channel, 869 or 915MH, half-duplex, 9600 baud, wideband transceiver modem module with a built-in ceramic antenna (Figure 5). The transceiver module operates at +5V, has 5mW transmit power and -106dBm receiver sensitivity.

Figure 6 shows the block diagram of the example system. Here, the EasyMX Pro for STM32 ARM Cortex M3 based microcontroller development board with STM32F107 microcontroller is used at the sensor station. UART output of the development board is fed to the TXD input of the DWA3 transmitter modem.

The equipment station is based on the low-cost and lower-performance EasyPIC Pro V7 development board with the PIC18F45K22 microcontroller on board. In this example, for simplicity and demonstration purposes, an LED is used and controlled by gesture at the equipment station. The UART input of the development board receives commands from the DWA3 modem. The LED is turned ON or OFF or flashed depending on the received gesture command.

The software was developed using the mikroC language. Figure 7 shows the command structure. The sensor station detects the following hand movements: left to right, right to left, top to bottom and bottom to top, and sends commands to the equipment station through the DWA3 transmitter modem.

The equipment station receives commands through the DWA3 in receive mode. The hand movements and corresponding LED actions are given in Listing 1:

Hand movement	Command sent	LED action
Left to right	ON	Turn ON
Right to left	OFF	Turn OFF
Top to bottom	FL2	Flash 2 times
Bottom to top	FL3	Flash 3 times

```
BEGIN/SENSOR_STATION
        Initialize UART
        Initialize Gesture board
DO FOREVER
        IF left to right movement detected THEN
                Send "ON$" to UART
        ELSE IF right to left movement detected THEN
                Send "OFF$" to UART
        ELSE IF top to bottom movement detected THEN
                Send "FL2$" to UART
        ELSE IF bottom to top movement detected THEN
                Send "FL3$" to UART
                ENDIF
        ENDDO
END/SENSOR_STATION


BEGIN/EQUIPMENT_STATION
Initialize UART
DO FOREVER
        Receive a command through UART
        IF "ON" received THEN
                Turn LED ON
        ELSE IF "OFF" received THEN
                Turn LED OFF
        ELSE IF "FL2" received THEN
                Flash LED 2 times
        ELSE IF "FL3" received THEN
                Flash LED 3 times
                ENDIF
        ENDDO
END/EQUIPMENT_STATION
```

Listing 1: Operation of the sensor and the equipment stations

The complete program listings of this simple example for both sensor and equipment stations are given in Figure 8. At the sensor station, the gesture board and the UART are initialised and the program enters an endless loop, waiting for gesture movements to be detected. Any valid movement is sent to the equipment station via the transmitter module. Notice that the

"$" character is used as the command terminator.

At startup of the equipment station, the UART is initialised to 9600 baud and the program goes into an endless loop, waiting for a command to be received through the UART. Received commands are decoded and the LED is turned ON, OFF or flashed either twice or three times. ●

```
// SENSOR STATION
#include "GestureDefs.h"
#include "Gesture.h"
sbit MGC_RST at GPIOA_ODR.B0;
sbit MGC_RDY_IN at GPIOD_IDR.B10;
sbit MGC_RDY_OUT at GPIOD_ODR.B10;
extern s_Gesture mGesture;
extern char raw_data[132];
char gest_evt;

void Send_Gesture_Command()
{
 gest_evt = (char) mGesture.DataOut.GestureInfo & 0xFF;
 if (gest_evt)

 {
 switch (gest_evt)

 {
 case 1: // unknown
                        break;
 case 2: // left to right
            UART1_Write_Text("ON$");
                        break;
 case 3: // right to left
            UART1_Write_Text("OFF$");
                        break;
 case 4: //up to down
            UART1_Write_Text("FL2$");
                         break;
 case 5: // down to up
            UART1_Write_TExt("FL3$");
                        break;
 }
 }
}

void main()
{
 GPIO_Digital_Output (&GPIOA_BASE, _GPIO_
PINMASK_0);
 GPIO_Digital_Input (&GPIOD_BASE, _GPIO_
PINMASK_10);
 MGC_RST = 0;
 I2C1_Init_Advanced(400000, &_GPIO_MODULE_I2C1_
PB67);
 Delay_Ms(100);
 getFWInfo();
 setEnableAllGestures();
 Delay_Ms(10);
 UART1_Init_Advanced(9600,_UART_8_BIT_DATA,_
UART_NOPARITY,
 _UART_ONE_STOPBIT,&_GPIO_MODULE_USART1_
PA9_10);
 while (1)
 {
 updateGestureData();
 Send_Gesture_Command();
 }
}

// EQUIPMENT STATION
#define LED PORTC.RC0

void Flash(unsigned char x)
{
 unsigned char i;
 for(i=0; i< x; i++)
 {
 LED = 1;
 Delay_Ms(1000);
 LED = 0;
 Delay_Ms(1000);
 }
}

void main()
{
 unsigned char buffer[10];
 ANSELC = 0;
 TRISC = 0;
 LED = 0;
 UART1_Init(9600);

 while(1)
 {
 if(UART1_Data_Ready() == 1)
 {
 UART1_Read_Text(buffer,"$",255);
 if(!strcmp(buffer, "ON"))LED = 1;
 else if(!strcmp(buffer, "OFF"))LED = 0;
 else if(!strcmp(buffer, "FL2"))Flash(2);
 else if(!strcmp(buffer, "FL3"))Flash(3);
 }
 }
 }
```

Listing 2: Program listing

COMMERCIAL PCB TECHNOLOGY IS ADVANCING POINT-OF-CARE MEDICAL DIAGNOSTICS

BY **DR DESPINA MOSCHOU**, RESEARCH FELLOW AT THE NANO GROUP, ELECTRONICS AND COMPUTER SCIENCE, UNIVERSITY OF SOUTHAMPTON

Lab-on-chip (LoC) is a technology that could revolutionise medical point-of-care diagnostics. Considerable research effort goes into innovating production technologies that will make commercial upscaling financially viable.

Printed circuit board (PCB) manufacturing techniques offer several prospects toward this goal. One approach is to use PCB techniques to manufacture Ag/AgCL reference electrodes, which are essential components of biosensors.

Recent research has structurally and electrically characterised prototype PCB-based Ag/AgCL reference electrodes. Scanning electronic microscopy and X-ray photoelectron spectroscopy were used to evaluate the electrode surface characteristics and determine the long-term stability and pH dependency of the prototypes. The results help compare fully-integrated PCB platforms with PCB pH sensors with the performance of discrete commercial reference electrodes.

Lab-On-Chip

LoC technology is seen as one of the most promising candidates for revolutionising medicine, owing to its inherent point-of-care capabilities which include advanced functionality, low sample volumes, rapid results and increased portability.

The current challenge facing LoC however is two-fold: one is the bottleneck surrounding its commercial adoption and the second is developing cost-effective means of upscaling production.

Semiconductor manufacturing techniques have been used for such diagnostic platforms but there is no standardised, reliable procedure to integrate microfluidics in an economically-viable way. Another alternative is to manufacture microfluidics with alternative processes and materials, such as glass, polymer or even paper substrates, but the challenge then is integrating the electronics. More recently, PCB manufacturing was adopted as an alternative and initial results are promising, facilitating effortless integration of electronics and microfluidics now referred to as lab-on-PCB platforms.

Several LoC components and prototypes have been demonstrated on PCBs, including chemical sensors, but to acquire sensitive and reliable sensor readings, stable and integrated reference electrodes are necessary. To date studies have focused on the end application rather than on investigating the physical and electrical characteristics of such PCB reference electrodes and it is this gap in the research that Newbury Electronics has filled.

At research level there are several means of depositing Ag on to substrates, but there is no viable commercial technique available to PCB makers. In the current work undertaken by Southampton University, Ag/AgCl pseudo-reference electrodes were successfully fabricated solely with commercially-available techniques that are routinely used in PCB manufacture for the application of Ag finish to standard PCBs. Research has now moved on to investigate the

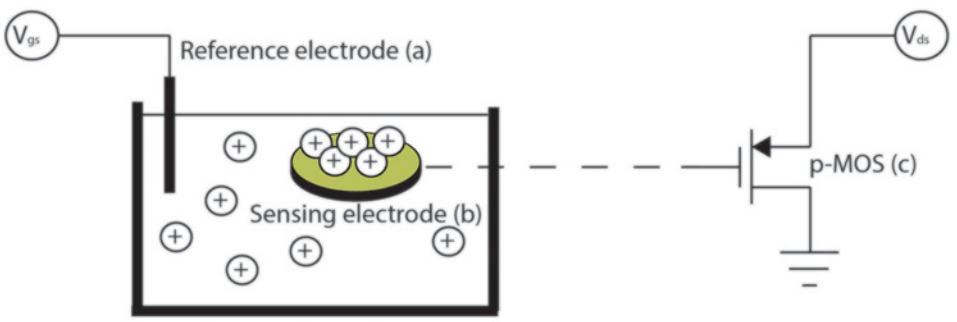

Figure 1: PCB-based biosensing platform setup

physical characteristics, electrical stability and pH dependence, whilst also benchmarking performance with commercially-available reference electrodes in a pH sensing experiment.

Experimental Activity

The prototype pseudo-reference electrodes consisted of an array of 80 vias of different diameters, ranging from 300µm to 1000µm. All prototyped reference electrodes were equipotential, and electrical connectivity was established through standard PCB headers soldered on to the boards.

Newbury Electronics then manufactured a prototype 2 x 4cm reference electrode platform, patterned the copper layers, formed the via holes and applied solder paste prior to immersion Ag coating of the patterned Cu electrodes. Vertical industrial polymer tanks were used for the mechanical agitation of the chemical solutions and constant vibration of the boards to ensure small-via conformal plating. The PCBs were then subjected to several other procedures to ensure conformally Ag-plated copper patterns, so the biological samples would not come into contact with copper, which is a well-known antimicrobial material and could unduly influence the assays.

The Ag-plated PCBs were subsequently immersed in NaOCl (bleach) solutions, producing an AgCl layer on top of Ag, forming the Ag/AgCl pseudo-reference electrodes. Various measurements and readings were taken using latest techniques and procedures, and the performance of the PCB pseudo-reference electrodes for chemical sensing was benchmarked against commercial reference electrodes and silver wires. To do so, an extended-gate PCB-based biosensing platform was used, to explore if it's possible to fully integrate PCB reference electrodes, sensors and microfluidics on a single platform.

The extended gate PCB sensors (Figure 1, point b) were remotely connected to the gate of a discrete transistor with a ribbon cable. The transistor drain was biased continuously at 0.5V and the source was connected to ground (0V), whilst the gate bias was applied to the respective reference electrodes (Figure 1, point a). The gate voltage was swept from -3V to 0V and the respective drain current-gate voltage transfer characteristics recorded. All experiments were performed at room temperature inside a Faraday cage to minimise the influence of external noise sources.

> PCB manufacturing has recently been adopted as an alternative and initial results are promising, facilitating an effortless integration of electronics and microfluidics now referred to as lab-on-PCB platforms

Proven Stability

The fabricated PCBs were physically characterised before and after NaOCl treatment to verify chlorination of the Ag layer; the results were found to be consistent with previous studies and confirmed successful chlorination of the vias. Electrode stability also required verification once the initial setup time has been allowed for, during which the electrodes have stabilised.

The PCB electrodes all demonstrated a very stable behaviour in the long term (drift < 1mV/24h) for pH of solutions ranging from 4 to 10, additionally featuring differences from commercial ones with drift as low as 1mV. Since the most common buffers used in biological analysis are close to neutral, the PCB reference electrodes were tested at pH = 7 over a long time, remaining stable for a total of 500 hours (20 days), a valuable spec for any electronics-based diagnosis tool that will be used in the field.

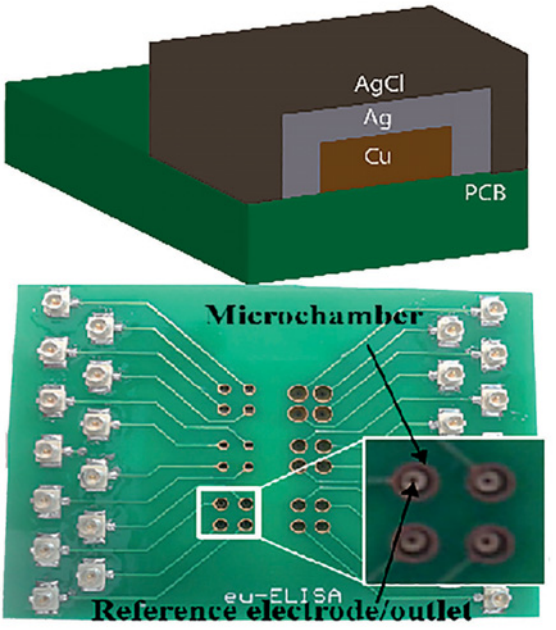

Figure 2: A PCB made by Newbury Electronics

The rationale behind this research is that the PCB reference electrodes being developed and tested are intended as components in integrated lab-on-PCB systems, hence will need to be as electrically stable when utilising biological buffers flowing through them as they are in immersion tests. To test this, a microfluidic delivery network was laser micro-machined and attached to a double-layer PCB with double-sided tape. The first layer comprises the reference electrodes and the second layer has cylindrical, gold-plated micro chambers.

HEPES buffer (pH = 7.4) was injected through an inlet, with the reference electrode via acting as a microchamber outlet, and the buffer continuously flowed through the reference electrode for 24 hours. The open-circuit voltage of the PCB reference electrodes against a commercial Ag/AgCl reference electrode was recorded, showing that even under constant flow the PCB reference electrodes demonstrated excellent stability.

Looking Ahead

This work with Newbury Electronics demonstrated that stable Ag/AgCl pseudo-reference electrodes can be fabricated solely by using techniques available at PCB manufacturers, opening the way for PCB-compatible component versions for biosensing platforms and complementing the development of PCB biosensors and lab-on-PCB systems.

Successful electrode chlorination was proven with surface characterisation techniques. Using FIB cross-section imaging, the AgCl layer was determined to be around 1.5µm thick.

The PCB reference electrodes demonstrated excellent long-term stability and, when combined with PCB pH sensors and tested, they showed sensitivity of 45.8mV/pH – comparable to commercial Ag/AgCl electrodes.

Looking ahead, the aim is to integrate such stable PCB-integrated reference electrodes to serve both as reference electrodes and fluidic outlets for PCB microfluidics in lab-on-PCB platforms that are currently under development to provide fully-integrated immunodiagnostic chips. ●

CURRENT PROJECT DEVELOPMENTS

Having verified the successful commercial fabrication of PCB reference electrodes, the project team is currently working on developing the PCB biosensor part and the integration process for a full lab-on-PCB platform.

On the PCB biosensor front, PCB gold-plated electrodes – made by Newbury Electronics – integrated with reference electrodes are exploited. The team is currently working on developing clinically relevant assays (IFN-gamma detection, glucose), evaluating and constantly improving sensor sensitivity, reliability and detection limit. A custom-made, versatile instrumentation board was developed and used to achieve this. On the lab-on-PCB integration front, a commercial process enabling mass manufacture of PCB microfluidics integrated with multi-layer PCB electronics has already been established with Newbury Electronics. It is understood that such a service is not currently provided by any other global PCB manufacturer.

PCB microfluidics are further investigated to explore the possibility of implementing passive pumping on lab-on-PCBs, with very promising results. This development would render cumbersome laboratory pumps obsolete, facilitating the application of diagnostic lab-on-PCBs at the point-of-care.

"When we started this project with Southampton University's Nanofabrication Centre, we expected that production of the electrodes would require specialist machinery. However, a prime objective was to use conventional methods. We were pleased to be able to devise a sequence of processes that fabricated a complex device, whilst using well understood individual manufacturing steps. We look forward to developing these methods further with the Nanofabrication Centre," said Philip King, Newbury Electronics's Managing Director.

PEAK® electronic design ltd
For more information or to place an order, contact us:
peakelec.co.uk 01298 70012 (+44 1298 70012)
PayPal
ZEN50 Zener Diode Analyser (inc. LEDs, TVSs etc)
New product!
Introducing the new *Atlas ZEN* (model ZEN50) for testing Zeners (including Avalanche diodes) and many other components.
- Measure Zener Voltage (from 0.00 up to 50.00V!)
- Measure Slope Resistance.
- Selectable test current: 2mA, 5mA, 10mA and 15mA.
- Very low duty cycle to minimise temperature rise.
- Continuous measurements.
- Single AAA battery (included) with very long battery life.
- Gold plated croc clips included.
- Can measure forward voltage of LEDs and LED strings too.
£39.00
£32.50+VAT
LCR45 LCR and Impedance Meter with Auto and Manual modes
New product!
Introducing a new powerful LCR meter that not only identifies and measures your passive components (Inductors, Capacitors and Resistors) but also measures complex impedance, magnitude of impedance with phase and admittance too! Auto and Manual test modes allow you to specify the test frequency and component type.
- Continuous fluid measurements.
- Improved measurement resolution: (<0.2µH, <0.2pF).
- Test frequencies: DC, 1kHz, 15kHz, 200kHz.
- Measure the true impedance of speakers and more.
- Great for hobbyists and professionals.
£90.00
£75.00+VAT
It's only possible to show summary specifications here. Please ask if you'd like detailed data. Further information is also available on our website. Product price refunded if you're not happy.

JTAG TECHNOLOGIES®

hardware testing & in-system device programming

tools or turnkey projects

01234 831212

sales@jtag.co.uk

www.jtag.com

ODU AMC® HIGH-DENSITY

Innovation in a **compact package**

SMALLER – LIGHTER – FASTER

ODU AMC High-Density is a robust miniature connector series that fulfills all the demands of the modern military equipment. The compact and lightweight connector solutions offer an excellent transmission performance, easy handling and high reliability.

- **Break-Away** for maximum safety
- **2** up to **40 contacts**
- Watertight – protection class **IP 68**
- **USB 2.0 + USB 3.0** data transfer
- **> 5,000 mating cycles durability**

ODU-UK Ltd.
Phone: +44 1509 266433
sales@odu-uk.co.uk
www.odu-uk.co.uk

ODU®
A PERFECT ALLIANCE.

AGGLUTINATION PHOTOMETRIC DETECTION WITH AN INTEGRATED MICROFLUIDIC SYSTEM

BY **NING YANG, TIANYUAN LV, ZHIYU ZUO, HANPING MAO** AND **CHANGHUA XIANG**
FROM JIANGSU UNIVERSITY, CHINA

The microfluidic chip is a modern way of analyzing preparation, reaction, separation and detection of liquids in biology, chemistry, medicine and other fields. It offers high detection speed and efficiency, low error rates and automation.

However, despite its usefulness, academics have found that it suffers from detection errors in certain conditions, and yet, to date, there have been no thorough analyses of these errors. We set out to research the error distribution model of immune aggregation microfluidic systems for different parameters, presented here.

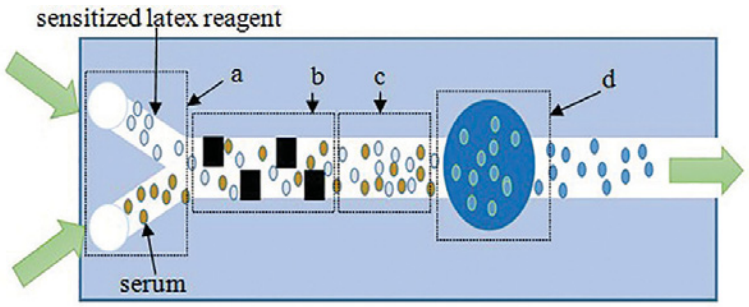

Figure 1: Microfluidic chip

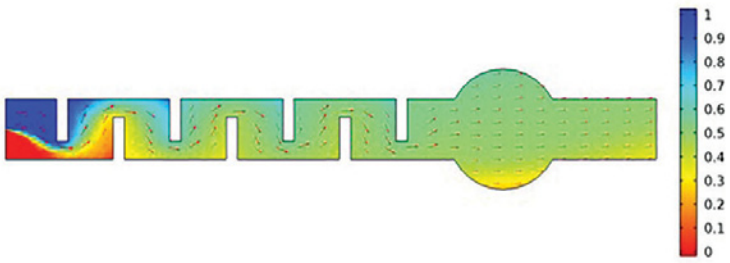

Figure 2: Microfluid mixing process in the microchannel

Microfluidic Chip Design

Since the channel of the microfluidic chip is so small, gravity and other Newtonian mechanics effects may be ignored. However, surface tension, repulsive force and other factors are main influences on the dynamic performance of the fluid, giving fluids an approximately laminar flow, which seriously hinders mixing of reactants and affects detection results. So, it is essential to design an efficient micro-mixer to ensure adequate biochemical reaction.

Current micro-mixers can be dynamic or static; the first accelerates the mixing process by using magnetic, electric and other type forces, and the other achieves mixing with barriers that 'channel' the fluid into the mixing chamber. The dynamic mixing method is highly efficient, but it requires external, powered facilities, such as a magnetic field generator. This makes the mixers large and bulky and hence not portable.

Figure 1 shows the chip, where 'a' is a Y-shaped sampling zone, 'b' the mixing zone and 'c' the reaction zone. Reagents enter the microfluidic chip from the sampling zone. When flowing, adequate mixing is achieved in the mixing zone, after which a full mixture is achieved in the final or reaction zone.

In this experiment, the sensitized latex reagent and serum are chosen for immunization agglutination reaction, after which visible agglutinators are formed. The corresponding detection operation is carried out in the photoelectric detection zone 'd' to determine the degree of reaction between the two fluids.

Figure 2 shows the mixing process, which was simulated with COMSOL Multiphysics 4.3. When the injection rate is 0.167mm/s, the structure leads to the two liquids' intense vertical flow, which accelerates mixing.

The chip was made using a method called 'imprinting', shown in Figure 3. First, a silicon or quartz mould is made, which is then press-bonded onto a substrate, forming the desired shape. Our chip (Figure 4) was made with the help of Suzhou Daya Electronics.

Detection Principle

In the presence of an electrolyte, particulate antigens (i.e. complete pathogenic micro-organisms or red blood cells, etc) can combine with antibodies and form small, visible agglutination pieces, a process known as “immune agglutination reaction”. We prepared a UV photometric detection experiment based on this process, using positive rheumatoid factor serum samples.

Different concentrations of the solution can absorb light of different wavelengths with distinct absorption efficiency. The optimal wavelength is the wavelength of absorbed light when the absorption efficiency is at a maximum, also called the resonant frequency lightwave.

In our experiment, the LED is connected to a precision light source (an instrument that provides various light wavelengths) – Ocean Optics HL-2000-HP-FHSA – while the detection device is connected to an Ocean Optics USB2000 spectrograph. The rheumatoid factor positive serums with titers of 20IU/mL, 30IU/mL, 40IU/mL, 50IU/mL and 60IU/mL react with the sensitized latex reagent respectively. Achieving optimum wavelength match is necessary before immune agglutination occurs. The results are shown in Table 1, where it can be seen that at a fixed wavelength, the concentration is higher and absorbance better; absorbance reaches its maximum at 580nm, 0.48Abs/ (IU/mL).

Design Of The Optical Path Detection Circuit

The detection device was designed to enhance the sensitivity of concentration detection and improve detection accuracy; see Figure 5, where ‘d’ is the photoelectric detection zone. During detection, this zone is covered with a lid to prevent liquid overflow.

The photosensitive surface of the photoelectric diode is attached to the glass bottom of the chip. We selected the LED to emit light of 580nm wavelength.

Figure 6 shows the detection system. The microfluidic chip is placed between the LED and photoelectric diode, connected to a sampling-drive pump, with velocity of 0.098μm/step and accuracy under 1%.

The LED emits light perpendicular to the chip. The sensitized latex reagent (made up of pure and surface inactive polystyrene 50nm latex particles) and the rheumatoid factor serum samples with different titers are placed into syringes. The detection circuit is connected to -10V and +5V power.

The system uses an STC15F2K60S2 as its microprocessor,

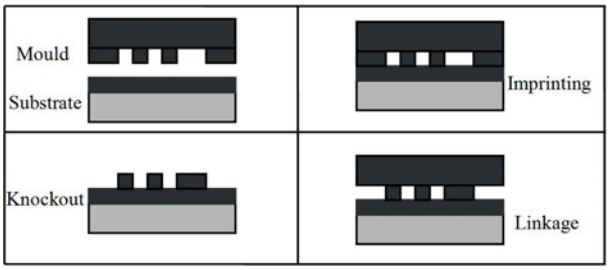

Figure 3: The microfluidic chip is fabricated using the imprint technique

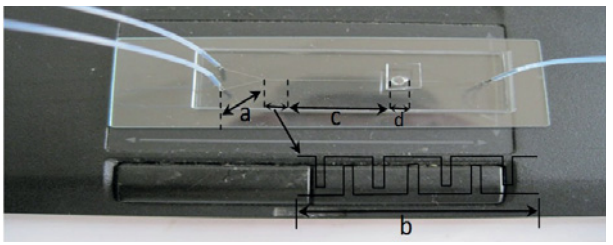

Figure 4: Microfluidic chip

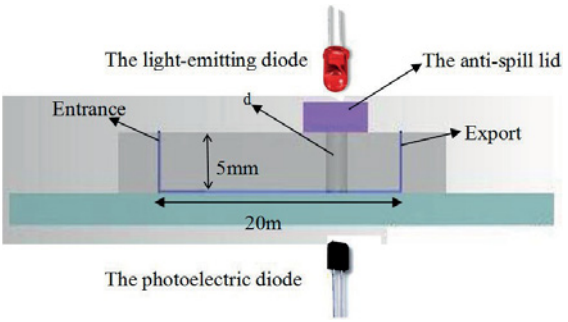

Figure 5: The design of the optical path detection circuit

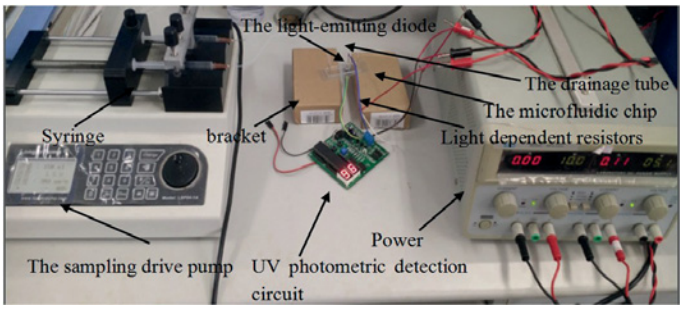

Figure 6: The UV photometric detection system

absorbtion / wavelength / concentration	400	460	520	580	640	700	760	820	880	940	1000
20	0.07	0.14	0.173	0.187	0.182	0.177	0.163	0.154	0.149	0.149	0.145
30	0.117	0.191	0.233	0.259	0.243	0.224	0.201	0.196	0.187	0.177	0.168
40	0.126	0.261	0.299	0.323	0.289	0.28	0.261	0.243	0.233	0.215	0.196
50	0.163	0.294	0.355	0.429	0.345	0.327	0.317	0.294	0.285	0.257	0.238
60	0.215	0.322	0.401	0.491	0.401	0.383	0.359	0.341	0.327	0.299	0.275

Table 1: Absorption spectrum of the rheumatoid factor in our experiment

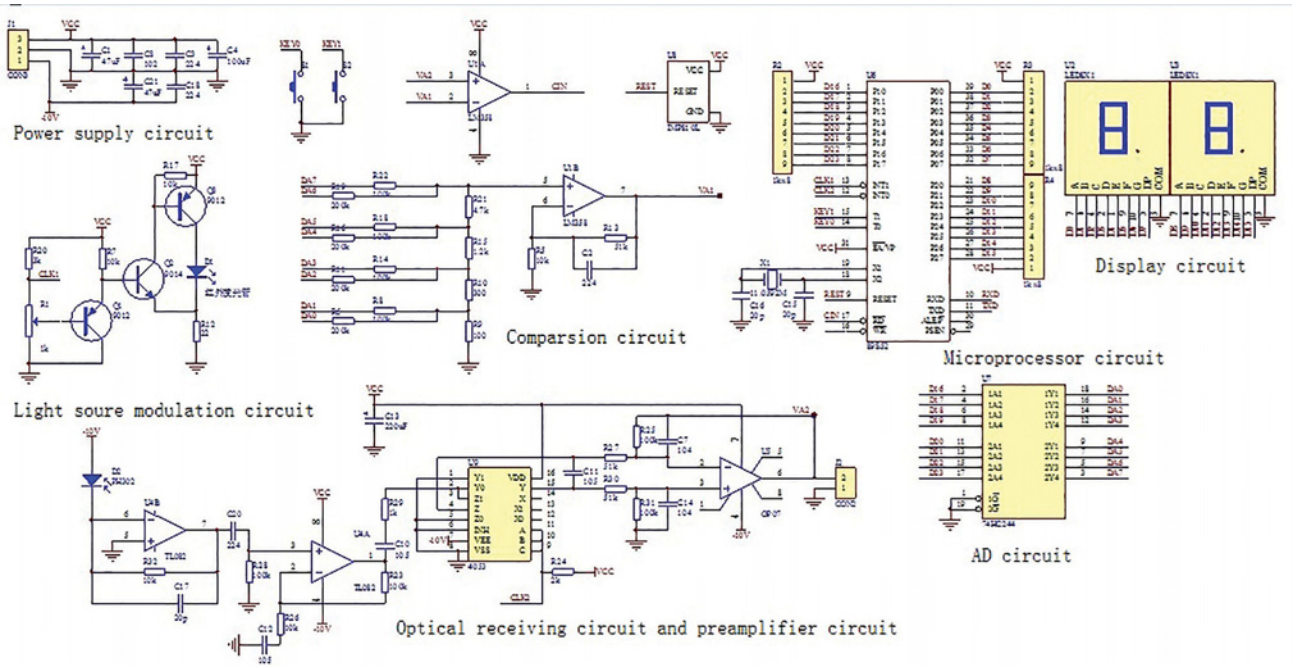

Figure 7: The analogue circuitry

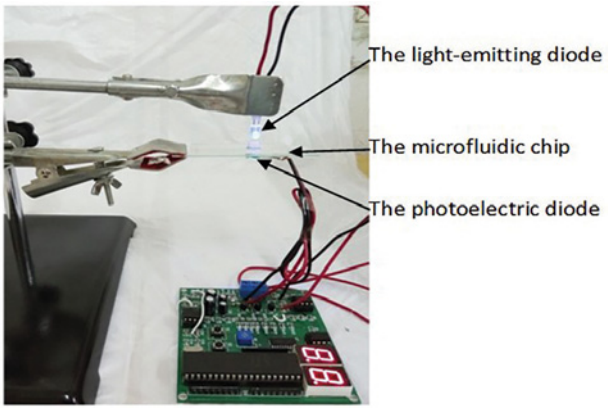

Figure 8: Optical path detection circuit

and the absorbance results can be displayed by the Nixie tube. The circuit includes a power supply, modulated light source, comparison module, optical receiving circuit, preamplifier, and a microprocessor and A/D converter; see Figure 7.

Unfortunately, the system suffers from noise: thermal, shot, produce-recombination and 1/f, the worst of which is the thermal noise. For these errors, there are two conventional solutions: hardware or software compensation methods. With hardware, a voltage-parallel negative feedback circuit preamplifier is placed in front of the processor. In software, a commonly used method is two-dimensional interpolation.

Error Analysis

Figure 9 shows the scatter diagram of the relationship between the concentration of the rheumatoid factor and immunoagglutination absorbance detection.

This was further analyzed with DPS statistical software. At the same time, the best linear fitting equation between the above two data sets is obtained by the curve fitting method. The correlation coefficient R of the two is 0.89 and the fractional error is about 20%.

The main sources of error are from the environment (such as temperature), sample's injection rate and agglutination reaction time. As the fractional error and correlation coefficient don't meet our requirements, it is essential to reach optimal parameters from four different error sources: temperature, pH value, sample injection rate and agglutination reaction time.

The experiment also shows that as the temperature increases, the fractional error of absorbance decreases; see Figure 10. The least square method is used to build the corresponding mathematical model of the absorbance fractional error that varies with temperature:

$$y = \begin{cases} 94.0526 - 4.9998 \cdot x^2 + 0.0665 \cdot x^3 & x \in [15,37] \\ 83.9607 - 4.5609 \cdot x + 0.0619 \cdot x^2 & x \in (37,45] \end{cases} \quad (1)$$

where x is temperature. The fractional error reaches minimum when the temperature is 37°C, and then increases with higher temperature. The main reason for this fractional error is the different number of bubbles created at different temperatures during absorbance detection, making 37°C the optimum reaction temperature before protein decomposition occurs.

pH Value Parameter Optimization

When photometric detection is carried out on the macro scale, the detection distortion caused by the change of pH can be ignored. But on the micro scale, microscopic agglutination distortion will seriously affect the results during photoelectric detection. So the influence of the pH value must be considered in the experiment.

We prepared seven sensitized latex reagents with pH values of 5.5, 6.0, 6.5, 7.0, 7.5, 8.0 and 8.5. The titer of the positive serum solution is 60IU/mL. The rheumatoid factor positive serum and sensitized latex reagents with different titers are injected into the microfluidic chip at the same time.

The absorbance fractional error varies with the pH value according to:

$$y = \begin{cases} 682.1896 - 191.12248 \cdot x + 15.3226 \cdot x^2 - 0.2325 \cdot x^3 & x \in [5.5, 7.5] \\ 146.9999 + 11.9507 \cdot x - 10.4908 \cdot x^2 + 0.8676 \cdot x^3 & x \in (7.5, 8.5] \end{cases} \quad (2)$$

where x is the pH value. As seen in Figure 11, the absorbance fractional error is lowest when pH is 7.5.

Agglutination Reaction Time Parameter Optimization

A certain time needs to transpire for full immune agglutination reaction. Taking measurements prematurely leads to errors due to the samples' inadequate reaction. Optimal reaction time can be determined by varying the absorbance detection.

During measurement, the concentration of antibodies in the positive serum is 60IU/mL, and absorbance values are checked every 20s under 600nm-wavelength light. When the absorbance reaches a steady value, we adopt it as standard.

We did 20 samples in total. The fractional error curve is drawn according to the recorded data, and the fractional error mixing index at different sample injection speeds at the exit of the mixing zone is determined with:

$$y = 228.3519 - 3.8116 \cdot x + 0.0159 \cdot x^2 \quad (3)$$

where x is the pH value. As shown in Figure 12, the absorbance became steady after 120s, so the time of the sample's moving from the mixed channel and into the detection port is 120s.

Injection Rate Parameter Optimization

In addition to all other parameters, optimum wavelength match is also necessary before the immune agglutination reaction.

The sample's injection rate is important for micro mixing: if too slow, mixing effectiveness decreases; if too high, inadequate reaction will lead to errors. Figure 14 shows the

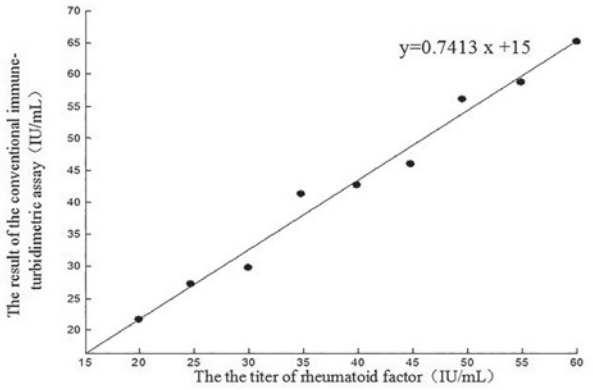

Figure 9: Regression analysis between the proposed and traditional methods

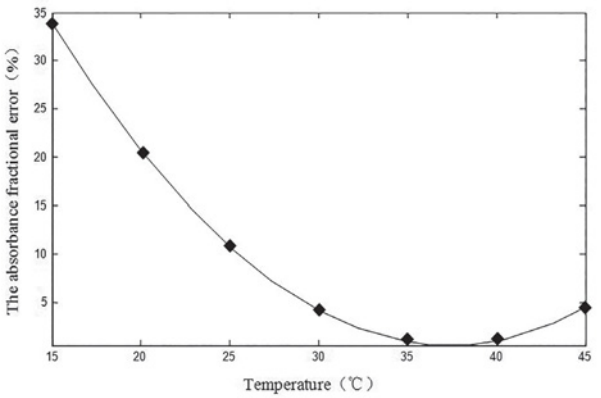

Figure 10: Absorbance fractional error varies with temperature

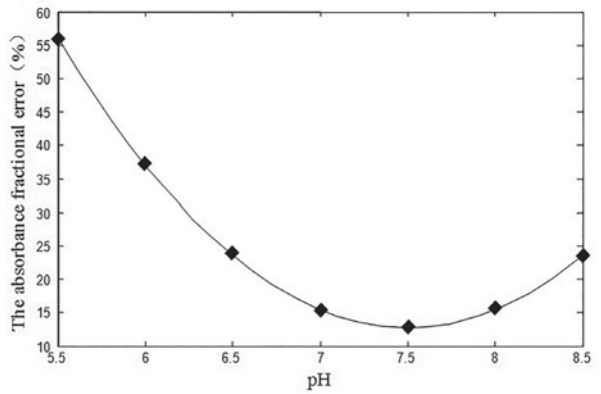

Figure 11: The absorbance fractional error varies with pH value

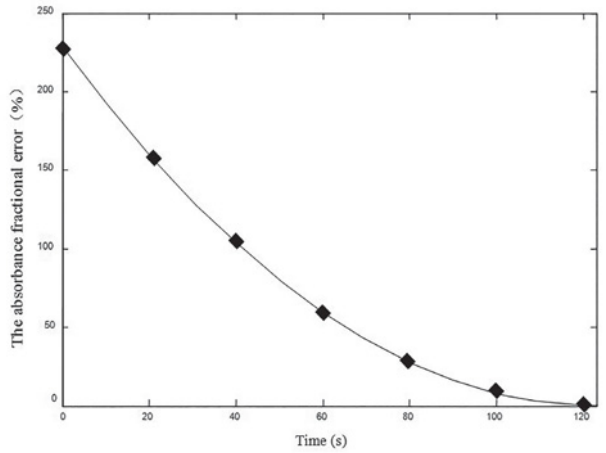

Figure 12: Absorbance fractional error varies with the reaction time

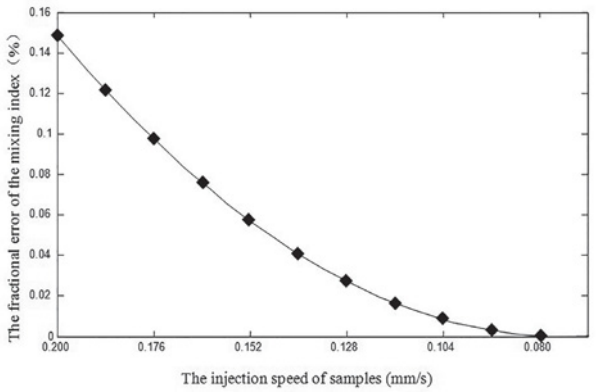

Figure 13: Fractional error mixing index at different sample injection speeds

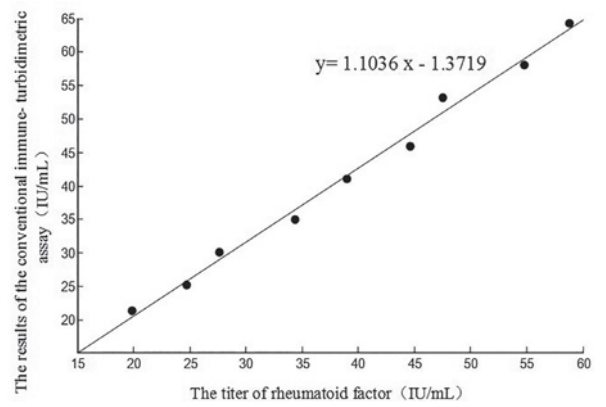

Figure 14: Fractional error mixing index at different injection speeds

fractional error mixing index at different sampling speeds at the exit of the mixing zone; mathematically this is:

$$M = \sqrt{\frac{1}{n}\sum_{i=1}^{n}(C_i - C_0)^2} \quad (4)$$

where C_i is the volume fraction at the specified plane node i, C_0 is the volume fraction when full uniformity is reached. As there are two sets of reagents that need to be mixed, the C_0 value is 0.5. Parameter n is the maximum number of discrete nodes in the specified plane. The mixture index M varies from 0 to 0.5, where 0 represents the intensive mixing between reagents.

From our experiment, it is clear that a full reaction is achieved in less than 120s. As shown in Figure 13, when the sampling speed decreases below 0.2mm/s, the concentration index becomes smaller. At a sampling speed of 0.08mm/s, liquids with different concentrations would mix intensely. The total time needed for the sensitized latex reagent and rheumatoid factor positive serum to pass through the mixing and reaction zones is 250s. This can be expressed as:

$$y = 0.0483 - 1.3527 \cdot x + 9.2708 \cdot x^2 \quad (5)$$

where x is the injection speed of samples.

Optimized Results

Figure 14 shows the immune response of the rheumatoid factor in the range 15-60IU/mL. When the concentration of the rheumatoid factor is higher than 70IU/mL, the absorption signal decreases.

Our experiment was repeated several times and mathematically this can be shown as:

$$y = \begin{cases} 0.1486 + 0.0315 \cdot x - 0.0032 \cdot x^2 & x \in [0,5] \\ 0.2126 + 0.0028 \cdot x & x \in (5,70] \\ 5.7032 \cdot 10^{-7} \cdot x^3 - 2.0364 \cdot 10^{-4} \cdot x^2 + 0.021743 \cdot x - 0.31127 & x \in (70,120] \end{cases} \quad (6)$$

where x is the titer of rheumatoid factor.

When the concentration of the rheumatoid factor is 5IU/mL, the designed detection system signal-to-noise (S/N) ratio is 3, making for 5IU/mL detectability. The macroscopic agglutination immunoassay detectability is 20IU/mL, where the detectability of the designed system drops to 75%.

Our study provides a theoretical guidance for a software-compensation algorithm and an error evaluation reference. However, there is also a disadvantage: the sampling-drive pump we used is too big, which goes against the principle of miniaturized equipment for ease of use and portability. But for now, if a smaller sampling-drive device is used, there's no guarantee that the sample introduction can be highly accurate. ●

FMicro NTC Miniature Thermistor Sensors

ATC Semitec's Fmicro miniature thermistor sensor has been designed primarily for use in medical applications.

Utilising thin-film technology combined with laser-trimming techniques, the Fmicro thermistor sensor is only 0.5mm diameter by 2.3mm long. It is designed around one of our smallest FT series thermistors, encapsulated in a polyimide tube and fitted with 38AWG insulated leads.

The Fmicro is accurate to ±0.2K at 37°C and is small enough to be incorporated within a catheter probe for internal body temperature measurement. Operating temperature range is -10/+70°C.

ATC Semitec Ltd,
Unit 14 Cosgrove Business Park,
Daisy Bank Lane, Anderton,
Northwich, Cheshire, CW9 6FY
Tel: 01606 871680
Fax: 01606 872938
E-mail: sales@atcsemitec.co.uk
Web: www.atcsemitec.co.uk

Now available in 0.3mm dia.

DKIH Compensated High Current Choke

- Compact size and light weight
- Open design for optimal cooling
- Wide temperature range
- Customer specific pin outs available

dkih.schurter.com

SCHURTER
ELECTRONIC COMPONENTS

RELEC
ELECTRONICS LTD

Trying to keep a low profile?

Ranging from 40W to 112.5W with convection cooling and up to 225W with forced air cooling. Relec Electronics has a range of open frame ac dc power supplies on a 4" x 2" footprint with a height profile of just 25.4mm for those designs where a low profile is critical. All feature high efficiency with low standby power consumption and a universal ac input. Single fixed outputs range from 12 to 48Vdc on the lower power units and 12 to 58Vdc on the 112.5/225W unit.

Approved to IEC, EN, UL 60950-1 2nd edition, class II safety standards, the 40W & 60W PSU's have an optional function ground enabling them to meet class I when this is connected. Hold up time is between 10 and 16ms; the outputs are fully protected against over voltage and short circuits.

These power supplies are ideally suited for telecom, datacom and a wide range of industrial applications. For further information on the 40W **MPE-S040**, 60W **MPE-T060** or 112.5/225W **ABC225** series, view the Relec website or contact us directly.

POWER DISPLAYS EMC

www.relec.co.uk

Tel: 01929 555800
e-mail: sales@relec.co.uk

MONITORING RESPIRATION WITH ACCELERATION SENSORS

BY **PIOTR BRATEK, PIOTR DZIURDZIA, IRENEUSZ BRZOZOWSKI, WOJCIECH GELMUDA, JACEK OSTROWSKI** AND **ANDRZEJ KOS** FROM AGH UNIVERSITY OF SCIENCE AND TECHNOLOGY IN KRAKÓW, POLAND

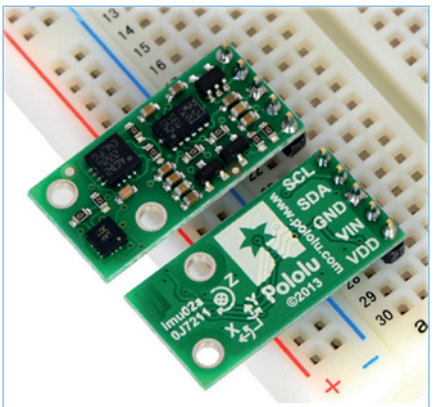

Figure 1: AltIMU-10 module

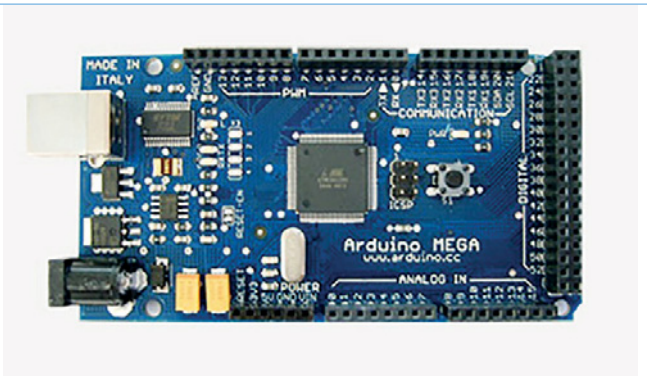

Figure 2: ArduinoMega evaluation board

Respiration is one of the most vital body parameters. Application-specific sensors and measurement methods, as well as advanced processing of collected data, are normally used to determine the state of patient's respiration.

There are various commercial devices that achieve this, such as sensors placed near the patient's nose or mouth, or even in the endotracheal tube. Very good results are achieved by measuring thoracic impedance, or heat energy from breath, with a temperature sensor. Some approaches are based on observing the patient, especially their chest movements, or the frequency of facial movements, and linking those to respiration parameters.

Analysing ECG signals, photo-plethysmography or blood pressure, radar, ultrasound and recording of acoustic waves are also known methods, all of which require sensitive equipment (such as microphones) and suitable signal processing algorithms and data collection and analysis software.

We propose an indirect method for respiration monitoring, based on an accelerometer sensor that counts breathing movements, in particular the reflexes generated by certain parts of the body, such as chest, arm and wrist.

The Setup

For our setup we used the readily-available AltIMU-10 module (Figure 1), which integrates sensors such as a digital barometer, 3-axis gyroscope, 3-axis accelerometer and 3-axis magnetometer, and the ArduinoMega development board (Figure 2).

The test system allows easy placement of sensors on the patient.

In addition to the chest, during breathing the diaphragm is also working, as well as the muscles under the lungs. Depending on the range of these motions, we can distinguish between a shallow or deep breath, so locating the sensor on the chest in the vicinity of the bridge is an obvious place, with additional sensors located on the shoulder and wrist.

Measurements were performed to estimate the error rate (noise) of the acceleration sensor, with each measurement lasting around two minutes.

We used LSM303D accelerometer that provides 256 units as equivalent to 1G gravity acceleration. It is in an LGA housing – land grid array (LGA) is a type of surface-mount IC packaging with pins on the socket rather than the IC – and it offers I2C and SPI communication ports. It can be powered between 2.16V and 3.6V, although the factory calibration is set to 2.5V.

Further acceleration measurements in three directions were taken at 20ms intervals.

To assess the sensor's error rate, the accelerometer was placed on a table; see Figure 3 for results corresponding to the x, y and z axes; they are in line with the acceleration sensor data sheets of the LSM303D.

With the sensor on the patient's chest, measurements

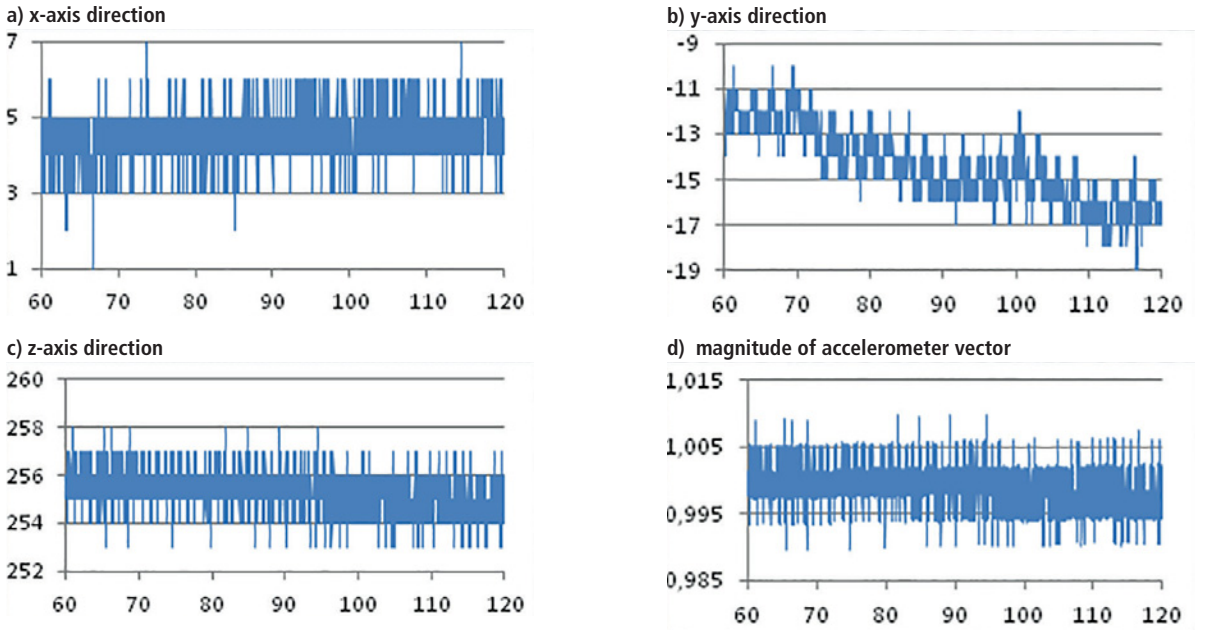

Figure 3: Indications of the sensor (1G/256) located on a table, for each axis direction (a, b, c) and magnitude of the accelerometer vector (d) against time (s)

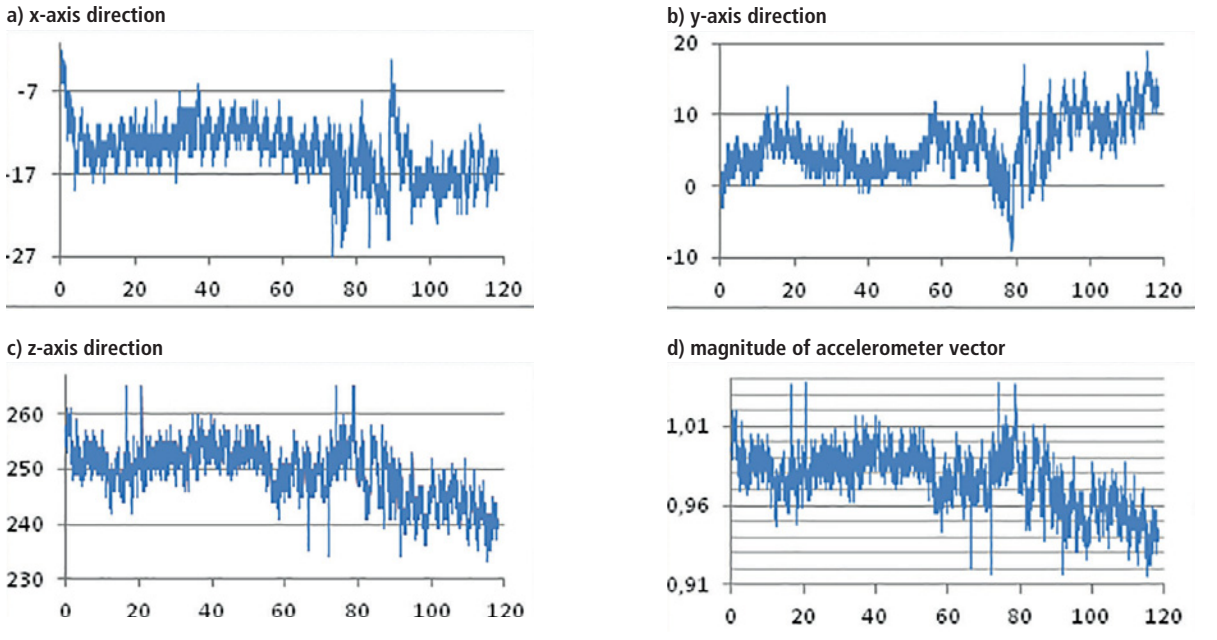

Figure 4: Indications of the sensor (1G/256) located on the chest, for each axis direction (a, b, c) and magnitude of accelerometer vector (d) against time (s)

were taken and the results are shown in Figure 4, with Figure 5 showing the general trend for the average of 50 measurements.

Then the sensor was placed on the patient's upper left arm, measurements taken and results shown in Figure 6, with Figure 7 showing the trend for 50 measurements.

The third set of measurements was taken with the sensor on the patient's left wrist; these are shown in Figure 9, whereas Figure 10 shows the average trend for 50 measurements.

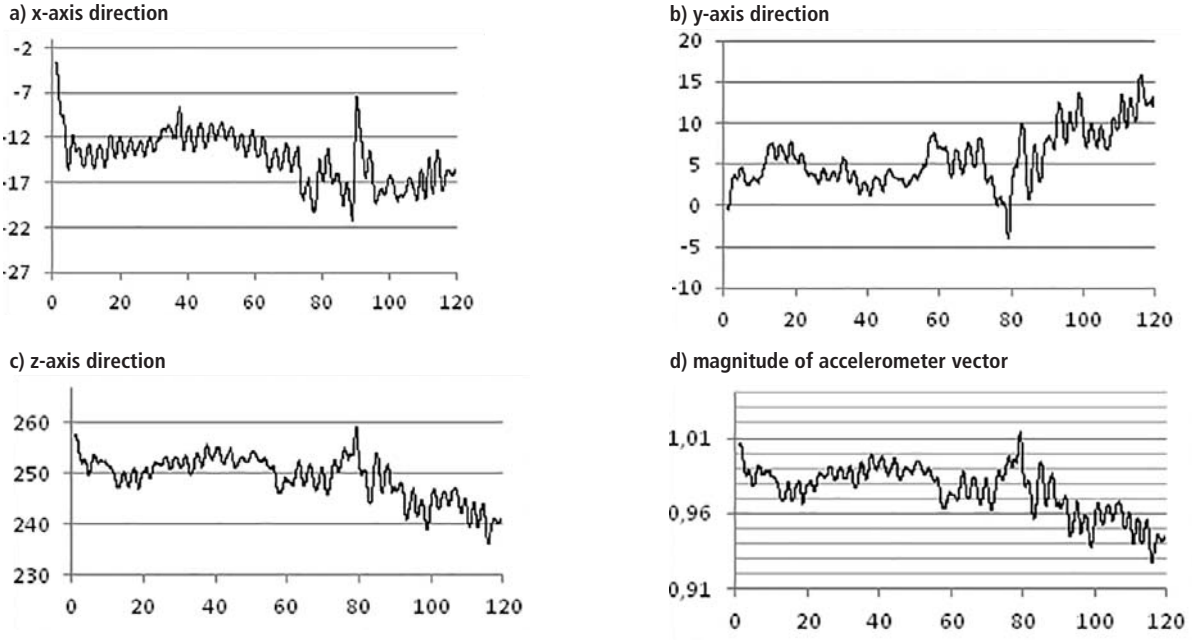

Figure 5: Trend lines composed of moving averages (period of 50 measurements) corresponding to data shown in Figure 4

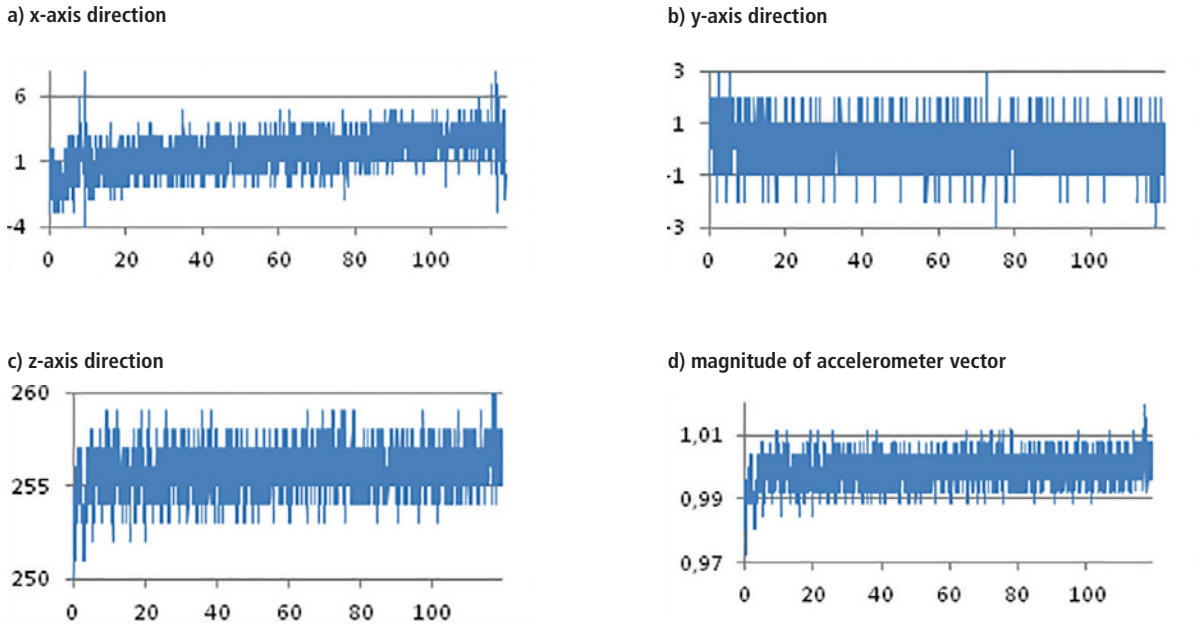

Figure 6: Indications of the sensor (1G/256) located on the upper left arm, for each axis direction (a, b, c) and the magnitude of accelerometer vector (d) against time (s)

Matlab Verification

Measurement verifications were performed with Matlab. Unfortunately, the filtering method used as a moving average for 50 measurements proved insufficient for accurate numerical determination of the number of breaths.

We then designed a digital low-pass filter, which was implemented as a quadruple averaging block for 32-length samples. The filter response was subjected to discretization, where 1 represents acceleration and 0 deceleration. At the end, the number of changes from acceleration to deceleration were determined in a 60s period. The collected results of the verification regarding data from Figures 6a, b and c are shown in Figures 10a, b and c, respectively.

In the case of sensor placement on the left wrist (Figures

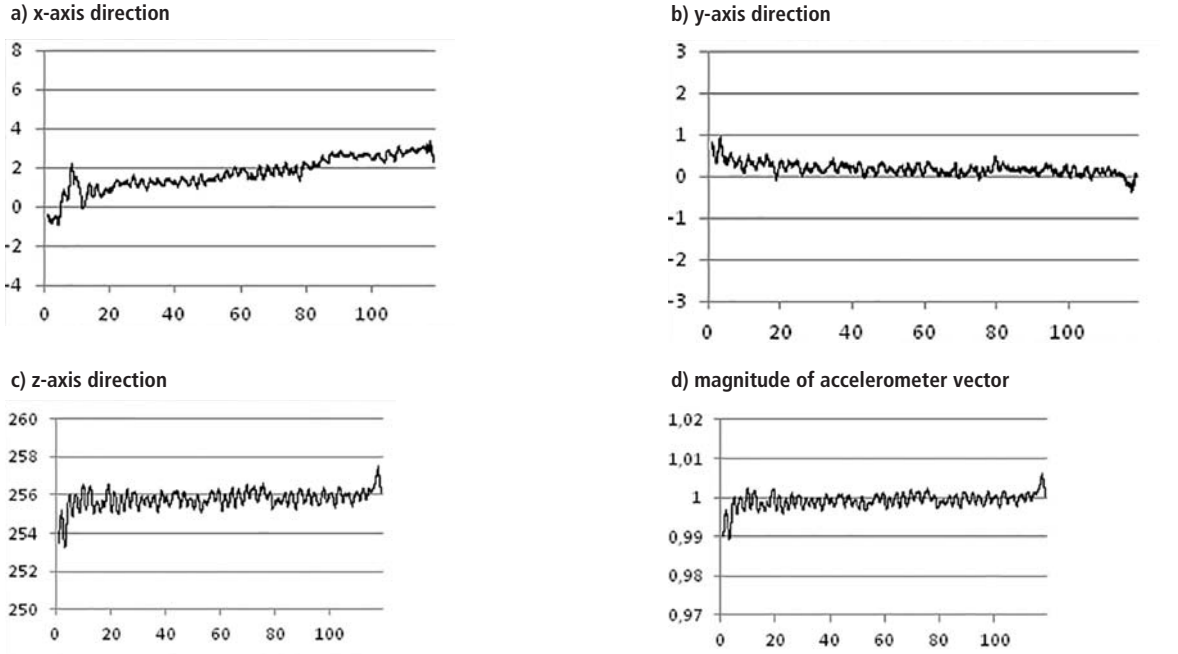

Figure 7: Trend lines based on moving averages (period of 50 measurements) corresponding to data shown in the Figure 6

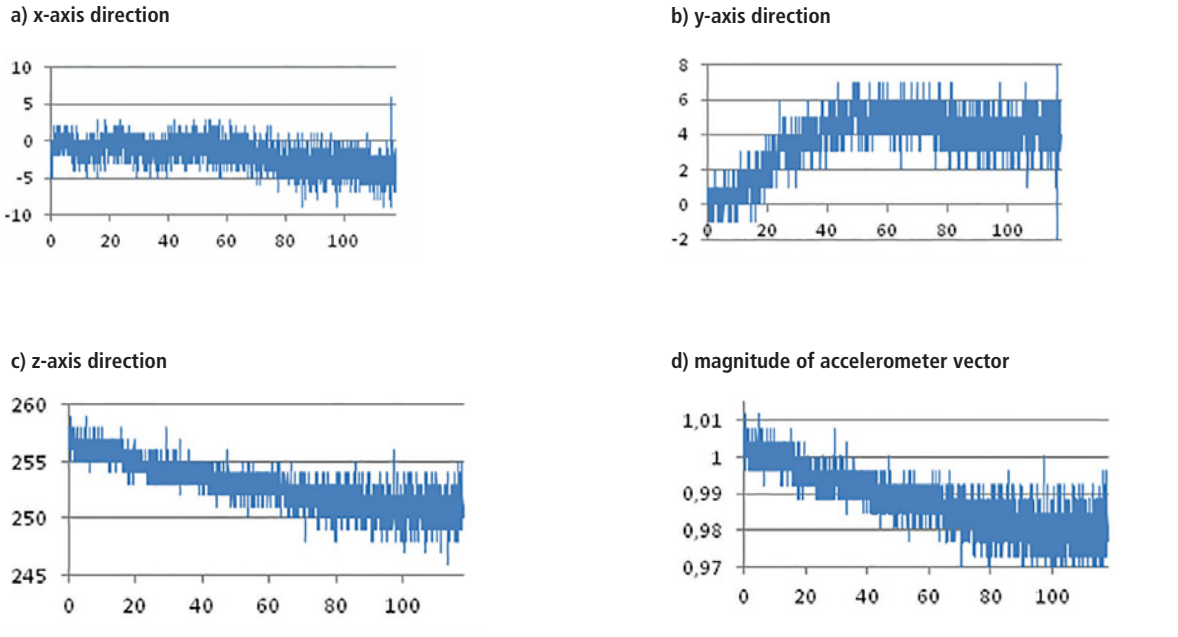

Figure 8: Indications of the sensor (1G/256) located on the upper left arm, for each axis direction (a, b, c) and magnitude of accelerometer vector (d) against time (s)

8 and 9), some periodic changes can be seen in two axes. Unfortunately, the recorded signals are at the same level as the noise generated by the sensor itself, which does not allow a reliable determination of the number of breaths.

Our tests confirm that an accelerometer sensor can be used for indirect estimation of breaths against time in respiration monitoring. The biggest change in sensor response was observed when the accelerometer is located closer to the chest than the wrist, for example.

Future Applications

For respiration monitoring, which so far has been very difficult to tackle with wearable electronics, our method is very likely to be adopted by the medical world. This is because the other

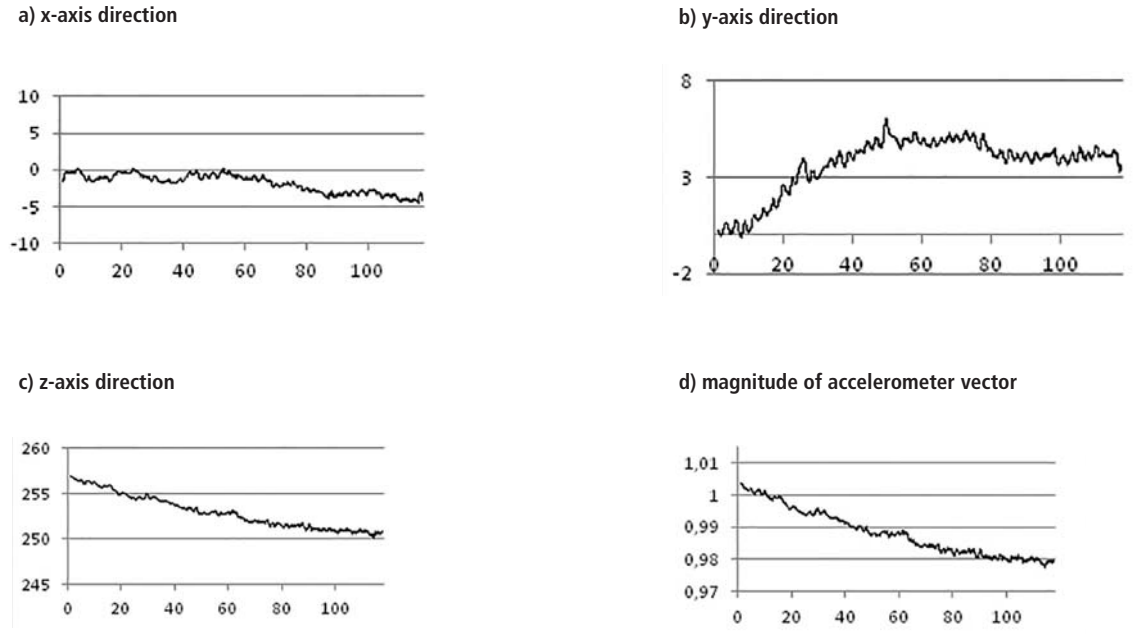

Figure 9: Trend lines composed of moving averages (period of 50 measurements)

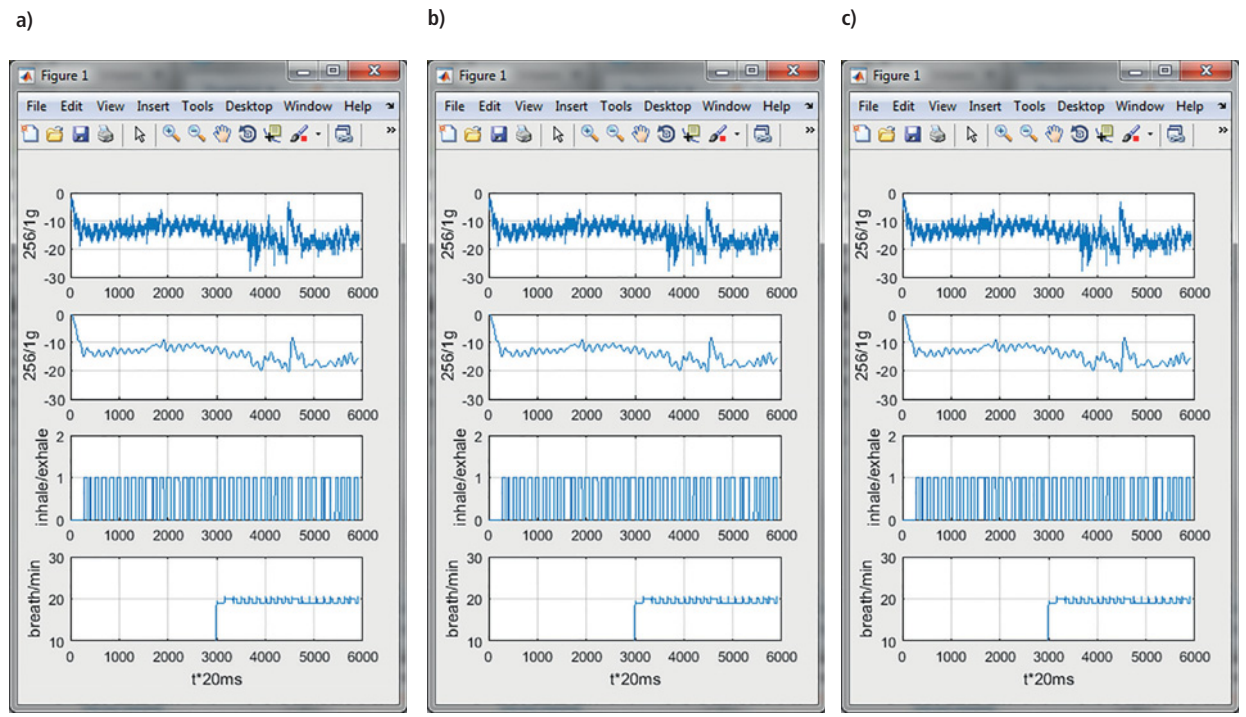

Figure 10: Verification of measurement data from Figure 4 with a low-pass filter

methods currently used and described at the beginning of this article need special and expensive equipment, as well as tolerant patients, although at this time they are more accurate too.

By using very small accelerometer with some radio transmission such as Bluetooth or Wi-Fi, a portable respiratory monitor could be used practically anywhere, from hospitals to rescue operations during accidents or disasters, and in situations where a medical service might be limited. ●

BEHIND EVERY SATISFIED CUSTOMER

THERE'S A DISTRIBUTOR YOU CAN COUNT ON

As the world's leading high-service distributor of electronics, automation and control, and tools and consumables, we do more than provide quality parts at competitive prices. With our dedicated customer service team who can offer technical support, as well as our award-winning design tools and resources, you can count on us for all the extra support you need.

uk.rs-online.com

CHOOSING THE RIGHT POWER FOR WIRELESS MEDICAL INSTRUMENTATION

BY **TONY ARMSTRONG**, DIRECTOR OF PRODUCT MARKETING FOR POWER PRODUCTS AT LINEAR TECHNOLOGY

As with many applications, low-power precision components have enabled rapid growth of portable and wireless medical instruments. However, unlike many other applications, medical products typically have much higher standards for reliability, run-time and robustness. As might be expected, much of this burden falls on the power system and its associated support components.

Medical products must operate properly and switch seamlessly between various power sources such as an AC mains outlet, battery backup and even harvested ambient energy sources. Furthermore, great lengths must be taken to protect against and tolerate faults, maximize operating time when powered from batteries and ensure that normal system operation is reliable whenever a valid power source is present.

A key area fueling growth in portable and wireless medical instrumentation is patient care, and specifically, the increased use of remote monitoring systems within the patient's own home. The key reason for this trend is purely economics as the increasing costs of keeping a patient in a hospital are proving prohibitive. As a result, portable monitoring systems must incorporate RF transmitters so any data gathered from the patient can be sent directly to a supervisory system in the hospital for immediate or later review by a physician.

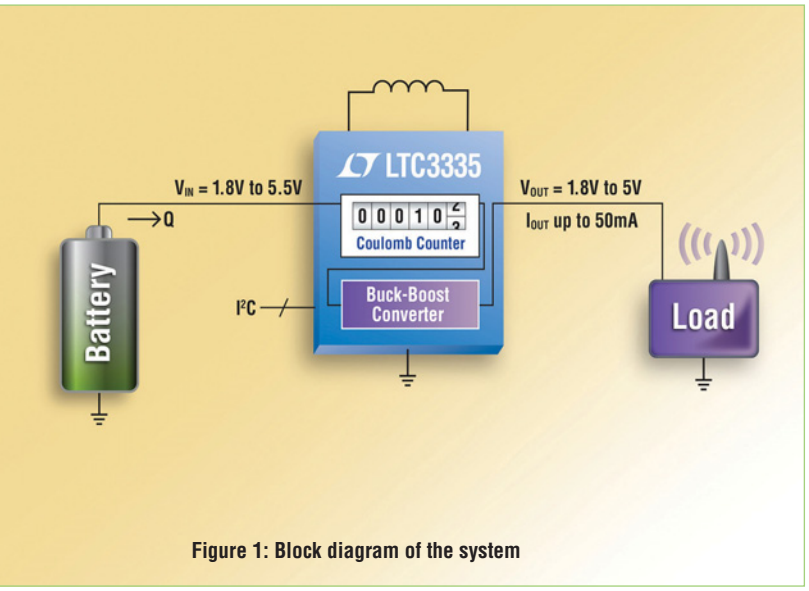

Figure 1: Block diagram of the system

Given this typical scenario, it is reasonable to assume that the cost of supplying appropriate medical instrumentation to patients for in-home use is more than offset by the cost of keeping them in hospital for observation. Thus, it is of paramount importance that equipment used by patients is reliable and fool-proof. As a result, manufactures and designers must ensure their products run seamlessly from multiple power sources whilst guaranteeing highly reliabile data transmissions. This requires great care in designing power management architectures, which have to be robust, flexible, compact and efficient.

Associated Pitfalls And Solutions

It is not unusual for a system designer to use linear regulators in a system that incorporates wireless transmission capability, since it minimizes EMI and noise emissions. Nevertheless, although switching regulators generate more noise than linear ones, their efficiency is far superior. Noise and EMI levels have proven to be manageable in many sensitive applications, as long as the switcher behaves predictably.

If a switching regulator switches at a constant frequency in normal mode, and the switching edges are clean and predictable with no overshoot or high frequency ringing, then EMI is minimized. Moreover, small package size and high operating frequency lead to a small, tight layout, which minimizes EMI radiation. Furthermore, if the regulator can be used with low ESR ceramic capacitors, both input and output voltage ripple can be minimized, further reducing noise in the system.

The main input power to today's feature-rich medical devices is usually 24V or 12V DC from an external AC/DC adapter. This voltage is then further reduced to either 5V and/or 3.xV rails using synchronous buck converters.

Still, the number of internal post-regulated power rails in these medical devices has increased while operating voltages have continued to decrease. Thus, many of these systems require 3.xV, 2.xV or 1.xV rails for powering low-power sensors, memory, microcontroller cores, I/O and logic circuitry. Furthermore, since medical device operation is often life-critical, they incorporate

battery backup to guarantee operation should the main power supply fail.

Traditionally, the lower-voltage rails have been supplied by step-down switching regulators or low-dropout regulators. However, these types of ICs do not capitalize on the battery cell's full operating range, thereby shortening potential battery run-time. Therefore, when a buck-boost converter is used (which can step voltages up or down from a variable input source), it will give access to the battery's full operating range. This increases operating margin and extends the battery run-time as more of the battery's useful capacity can be accessed, especially as it nears the end of its discharge profile.

DC/DC Solutions

It is clear that a DC/DC converter solution that solves the primary cell system application requirements, as well as the associated issues already discussed, should have the following attributes:

- Buck-boost power conversion architecture with wide input voltage range to regulate the output voltage through a variety of battery-powered sources and their associated voltage ranges.
- Ultra-low quiescent current, both in operating mode and shutdown, to increase battery run-time.
- The ability to efficiently power system rails.
- Capably count Coulombs accurately, without significantly affecting IC quiescent current (battery consumption) to determine battery state of charge.
- Current limiting to attenuate inrush currents thus protecting the cells.
- Small size, light weight and low profile footprints.
- Advanced packaging for improved thermal performance and space efficiency.

A recently introduced product by Linear Technology, the nanopower LTC3335 buck-boost converter with integrated Coulomb counter, has all these attributes. The device was designed for primary battery applications that need really low quiescent current and need to monitor remaining battery capacity, or where potential battery component or load leakage may be detected by the Coulomb counter as a check for system faults; see Figure 1.

> Small package size and high operating frequency can provide small, tight layout, which minimizes EMI radiation

The LTC3335 is a nanopower, high efficiency, synchronous buck-boost converter with onboard precision Coulomb counter that delivers up to 50mA of continuous output current. With only 680nA of quiescent current and programmable peak input currents from 5mA to 250mA, the device is suited to a wide variety of low-power battery applications, such as those found in battery-backed-up, portable, health-monitoring systems. Its 1.8-5.5V input range and eight user-selectable outputs between 1.8V and 5V provide regulated output supplies with an input voltage above, below or equal to the output.

In addition, the device's integrated precision (±5%) battery discharge Coulomb counter provides accurate monitoring of accumulated battery discharge in long-life non-rechargeable battery-powered applications, which in many cases have extremely flat battery discharge curves.

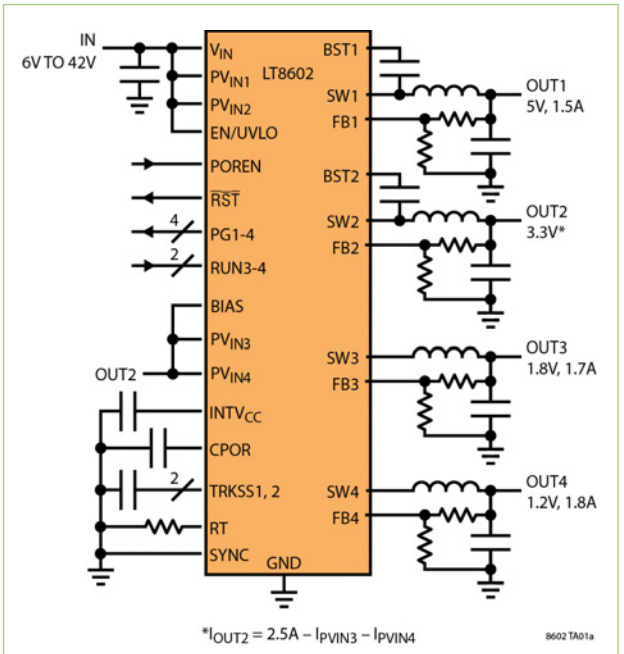

Figure 2: LT8602 delivers 5V, 3.3V, 1.8V and 1.2V outputs

Several Voltage Rails

Another way to get a combination of low voltages rails from a DC input of 24V or 12V is to use a high-voltage DC/DC converter with multiple output capabilities. So Linear Technology developed a four-output monolithic synchronous buck converter, the LT8602. Its 3-42V input voltage range makes it ideal for medical applications. As shown in Figure 2, its quad-channel design combines two high-voltage 2.5A and 1.5A channels with two lower-voltage 1.8A channels to deliver four independent outputs with voltages as low as 0.8V, enabling it to drive the lowest voltage microprocessor cores currently available.

Its synchronous rectification topology delivers up to 94% efficiency, while Burst Mode operation keeps quiescent current under 30µA (all channels on) in no-load standby conditions, making it ideal for battery-operated systems.

For noise-sensitive applications, the LT8602 with a small external filter can utilize its pulse-skipping mode to minimize switching noise and meets the CISPR25, Class 5 EMI requirements; it can be used readily in systems incorporating wireless data transmission.

The LT8602's switching frequency can be programmed from 250kHz to 2MHz and can be synchronized throughout

the full range. Its 60ns minimum 'on' time enables 16VIN to 2.0VOUT step-down conversions on the high-voltage channels with a 2MHz switching frequency. Since the high-voltage VOUT2 channel feeds the two low-voltage channels (VOUT3 and VOUT4), these deliver outputs as low as 0.8V whilst also switching at 2MHz, offering a very compact (~ 25mm x 25mm single-sided) quad output solution, as shown in Figure 3. In addition to minimizing the solution footprint, the LT8602's 2MHz switching frequency enables designers to avoid critical noise-sensitive frequency bands. Each channel of the LT8602 maintains a minimum dropout voltage of only 200mV (@1A) under all conditions, enabling it to excel in scenarios such as automotive cold-crank. Programmable power-on reset and power-good indicators for each channel help ensure overall system reliability.

The LT8602's 40-lead thermally-enhanced 6mm x 6mm QFN package and high switching-frequency keeps external inductors and capacitors small, providing a compact, thermally-efficient footprint. In addition, unique design techniques and a new high-speed process technology enable high efficiency over a wide input voltage range and the LT8602's current-mode topology enables fast transient response and excellent loop stability. ●

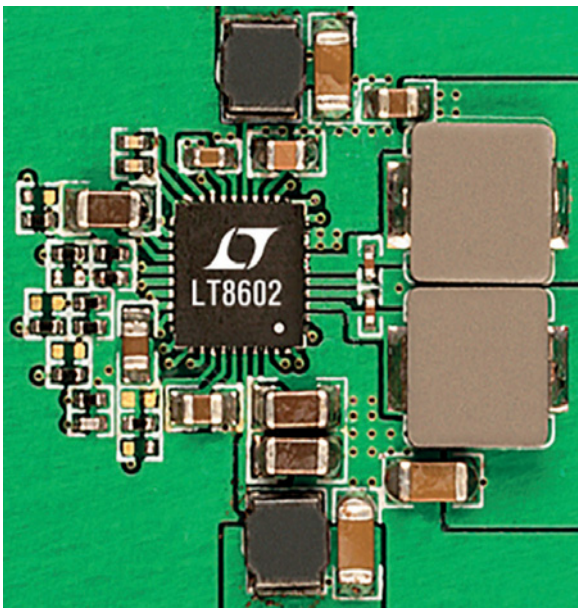

Figure 3: LT8602 quad-output footprint

HP 34401A Digital Multimeter 6 ½ Digit

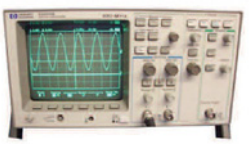

HP 54600B Oscilloscope Analoque/Digital Dual Trace 100MHZ

LAMBDA GENESYS	PSU GEN100-15 100V 15A Boxed As New	£325
LAMBDA GENESYS	PSU GEN50-30 50V 30A	£325
HP34401A	Digital Multimeter 6.5 digit	£275-£325
HP33120A	Function Generator 100 microHZ-15MHZ	£260-£300
HP53131A	Universal Counter 3GHZ Boxed unused	£500
HP53131A	Universal Counter 225MHZ	£350
HP54600B	Digital Oscilloscope 100MHZ 20MS/S	from £75
IFR 2025	Signal Generator 9kHz - 2.51GHZ Opt 04/11	£900
Marconi 2955B	Radio Communications Test Set	£800
R&S APN62	Syn Function Generator 1HZ-260KHZ	£195
Fluke/Philips PM3092	Oscilloscope 2+2 Channel 200MHZ Delay etc	£250
HP3325A	Synthesised Function Generator	£195
HP3561A	Dynamic Signal Analyser	£650
HP6032A	PSU 0-60V 0-50A 1000W	£750
HP6622A	PSU 0-20V 4A Twice or 0-50V 2A Twice	£350
HP6624A	PSU 4 Outputs	£350
HP6632B	PSU 0-20V 0-5A	£195
HP6644A	PSU 0-60V 3.5A	£400
HP6654A	PSU 0-60V 0-9A	£500
HP8341A	Synthesised Sweep Generator 10MHZ-20GHZ	£2,000
HP83731A	Synthesised Signal Generator 1-20GHZ	£1,800
HP8484A	Power Sensor 0.01-18GHZ 3nW-10uW	£75
HP8560A	Spectrum Analyser Synthesised 50HZ - 2.9GHZ	£1,250
HP8560E	Spectrum Analyser Synthesised 30HZ - 2.9GHZ	£1,750
HP8563A	Spectrum Analyser Synthesised 9KHZ-22GHZ	£2,250
HP8566B	Spectrum Analsyer 100HZ-22GHZ	£1,200
HP8662A	RF Generator 10KHZ - 1280MHZ	£750
Marconi 2022E	Synthesised AM/FM Signal Generator 10KHZ-1.01GHZ	£325
Marconi 2024	Synthesised Signal Generator 9KHZ-2.4GHZ	£800
Marconi 2030	Synthesised Signal Generator 10KHZ-1.35GHZ	£750
Marconi 2305	Modulation Meter	£250
Marconi 2440	Counter 20GHZ	£295
Marconi 2945	Communications Test Set Various Options	£2,500
Marconi 2955	Radio Communications Test Set	£595
Marconi 2955A	Radio Communications Test Set	£725
Marconi 6200	Microwave Test Set	£1,500
Marconi 6200A	Microwave Test Set 10MHZ-20GHZ	£1,950
Marconi 6200B	Microwave Test Set	£2,300
Marconi 6960B with	6910 Power Meter	£295

MARCONI 2955B Radio Communications Test Set

FLUKE/PHILIPS PM3092 Oscilloscope 2+2 Channel 200MHZ Delay TB, Autoset etc

Tektronix TDS3012	Oscilloscope 2 Channel 100MHZ 1.25GS/S	£450
Tektronix 2430A	Oscilloscope Dual Trace 150MHZ 100MS/S	£350
Tektronix 2465B	Oscilloscope 4 Channel 400MHZ	£600
Cirrus CL254	Sound Level Meter with Calibrator	£40
Farnell AP60/50	PSU 0-60V 0-50A 1KW Switch Mode	£195
Farnell H60/50	PSU 0-60V 0-50A	£500
Farnell B30/10	PSU 30V 10A Variable No Meters	£45
Farnell B30/20	PSU 30V 20A Variable No Meters	£75
Farnell XA35/2T	PSU 0-35V 0-2A Twice Digital	£75
Farnell LF1	Sine/sq Oscillator 10HZ-1MHZ	£45
Racal 1991	Counter/Timer 160MHZ 9 Digit	£150
Racal 2101	Counter 20GHZ LED	£295
Racal 9300	True RMS Millivoltmeter 5HZ-20MHZ etc	£45
Racal 9300B	As 9300	£75
Black Star Orion	Colour Bar Generator RGB & Video	£30
Black Star 1325	Counter Timer 1.3GHZ	£60
Ferrograph RTS2	Test Set	£50
Fluke 97	Scopemeter 2 Channel 50MHZ 25MS/S	£75
Fluke 99B	Scopemeter 2 Channel 100MHZ 5GS/S	£125
Gigatronics 7100	Synthesised Signal Generator 10MHZ-20GHZ	£1,950
Panasonic VP7705A	Wow & Flutter Meter	£60
Panasonic VP8401B	TV Signal Generator Multi Outputs	£75
Pendulum CNT90	Timer Counter Analyser 20GHZ	£750
Seaward Nova	PAT Tester	£95
Solartron 7150	6 1/2 Digit DMM True RMS IEEE	£65
Solartron 7150 Plus	as 7150 plus Temp Measurement	£75
Solatron 7075	DMM 7 1/2 Digit	£60
Solatron 1253	Gain Phase Analyser 1mHZ-20KHZ	£600
Tasakago TM035-2	PSU 0-35V 0-2A 2 Meters	£30
Thurlby PL320QMD	PSU 0-30V 0-2A Twice	£160-£200
Thurlby TG210	Function Generator 0.002-2MHZ TTL etc Kenwood Badged	£65

STEWART OF READING

17A King Street, Mortimer, near Reading, RG7 3RS

Telephone: **0118 933 1111** Fax: **0118 9331275**

USED ELECTRONIC TEST EQUIPMENT

Check website **www.stewart-of-reading.co.uk**

Working at the cutting edge of technology

Signal generation, analysis and phase noise test for demanding requirements

When working at the cutting edge of technology, you shouldn´t waste your time with inferior tools. Rely on measuring instruments evolved in the spirit of innovation and based on industry-leading expertise.

Instruments like the R&S®SMW200A vector signal generator, the R&S®FSW signal and spectrum analyzer and the R&S®FSWP phase noise tester. Each is at the crest of today´s possibilities.

See for yourself at
www.rohde-schwarz.com/ad/highend

ROHDE&SCHWARZ

ANALYZING MOBILE PHONE ELECTROMAGNETIC RADIATION

LEVENT SEYFI, **ERCAN YALDIZ** AND **CAN NACAROĞLU** FROM SELÇUK UNIVERSITY IN TURKEY EXPLORE THE VARIOUS LEVELS OF ELECTROMAGNETIC RADIATION EMITTED BY MOBILE PHONES IN DIFFERENT CONDITIONS

Figure 1: Garmin eTrex handheld GPS device

Figure 2: Narda EMR-300 electromagnetic radiation measurement device

Wireless has become an indispensible part of communicating. It all started with the walkie-talkies of yesteryear but today most people own a mobile phone. It is almost necessary to have one from an early age, as parents try to keep an eye on their children.

In turn, the rise of the mobile phone and its ubiquity have had a detrimental effect on the PC since any application previously handled by a computer – such as Internet browsing, social networks, sending and receiving e-mails, office software and so on – are now easily carried out by a smartphone.

Mobile Phone Communication

To communicate, mobile phones connect to a network of base stations. These base stations work continuously and since they can only serve a limited number of mobile phones, more than one have to be used.

Base stations are typically mounted on standalone towers, building rooftops or disguised inside advertisement billboards and placards. So, with their prevalence and constantly-on operation, they do radiate electromagnetic (EM) emissions all the time.

Mobile-phone radiation levels and that of base stations are determined by international organizations, especially as

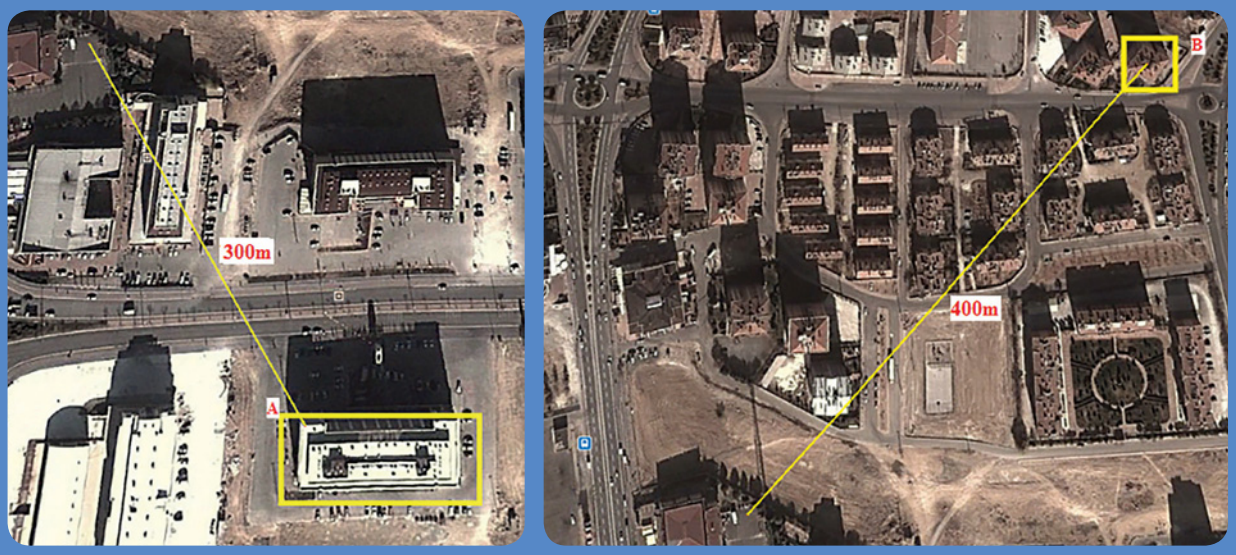

Figure 3: Building locations of (left) 300m and (right) 400m from the base station

radiation impacts human health and quality of life. In 1998, the International Commission on Non-Ionizing Radiation Protection (ICNIRP) published a report, establishing upper limits of electric field intensities for 900MHz and 1800MHz to be 41.25 and 58.34V/m respectively. Additionally, for the 3G-service-using 2100MHz this figure is 61V/m. It has been determined that RF systems with radiation levels below these limits are not harmful.

Project Setup

In this work, we set out to determine the EM radiation of mobile phones and base stations in different operating conditions, with some measurements taken inside enclosed spaces such as lifts and cars, and others in open areas. We analysed EM radiation at different operational times, such as when calling from a mobile phone, speaking, and sending texts, and also measured radiation from base stations in relation to distance.

Being based in Konya, Turkey, we established the coordinates for our measurement points with a Garmin eTrex GPS device, shown in Figure 1. European Datum 1950 for the international connection of geodetic networks was used as our reference. EM radiation values were measured with a Narda EMR-300 radiation meter, see Figure 2, using an electric field probe to measure radiation in the range of 100kHz to 3GHz, and displaying the values in V/m. Measurements can be taken in different modes, such as average, maximum and instantaneous.

The EMR-300 measurement device refreshes measurement values on its display every two seconds for six minutes. The maximum mode provides the maximum value of all measurements during that time, whereas the average mode provides the averaged value of all measurements, and instantaneous mode provides the momentary value of a measurement.

Measurements In Enclosed Spaces

We measured EM radiation of a mobile phone when speaking in a lift inside two buildings, as shown in Figure 3, situated at different distances from their respective base station.

For these measurements, we used the radiation meter in maximum mode; see the results in Table 1.

The results confirm that speaking with a mobile phone inside a lift creates more EM radiation. Inside the lift, the connection between base station and mobile phone is weakened because the metallic enclosure attenuates EM waves, so the mobile phone has to increase its output power to maximum to keep its connection.

Table 2 shows the maximum radiation for speaking into a mobile phone from inside a car. The meter was used in average mode to measure EM radiation of a mobile phone in standby; this was recorded to be 0.22V/m. Inside the car this value was 18.14V/m and 11.08V/m outside it.

The connection between a mobile phone and base station is

Location	Out of lift (V/m)	In lift (V/m)
Point A	3.4	22.82
Point B	5.82	26.20

Table 1: Measured maximum values while speaking using a mobile phone in a lift

		Measurement value (V/m)
Averaged EM radiation while mobile phone is in standby mode		0.22
Maximum radiation value during speaking	out a car	11.08
	in a car	18.14

Table 2: Measured values inside and outside a car

Conditions	Instantaneous value measurements (V/m)
Calling	11 - 23
Speaking	5 - 15
Sending SMS	3 - 8

Table 3: EM radiation measurement values whilst calling, speaking and sending SMS

	2G speaking (V/m)	3G speaking (video calling) (V/m)
1st point	1.38	2.96
2nd point	2.86	5.33

Table 4: The measurement values while speaking via 2G and 3G (video calling)

	Averaged measurements (V/m)
Point 1 (9th floor (top one) of building A)	0.68
Point 2 (5th floor of building A)	0.16
Point 3 (ground floor of building A)	0.13
Point 4 (last floor of building B)	4.73

Table 5: Measured EM radiation values for different building locations

Distance to the base station (m)	Average EM radiation (V/m)
0	1.38
20	1.67
40	1.86
60	2.07
80	2.20
100	1.96
120	1.16

Table 6: Measured EM radiation values versus distance to the base station

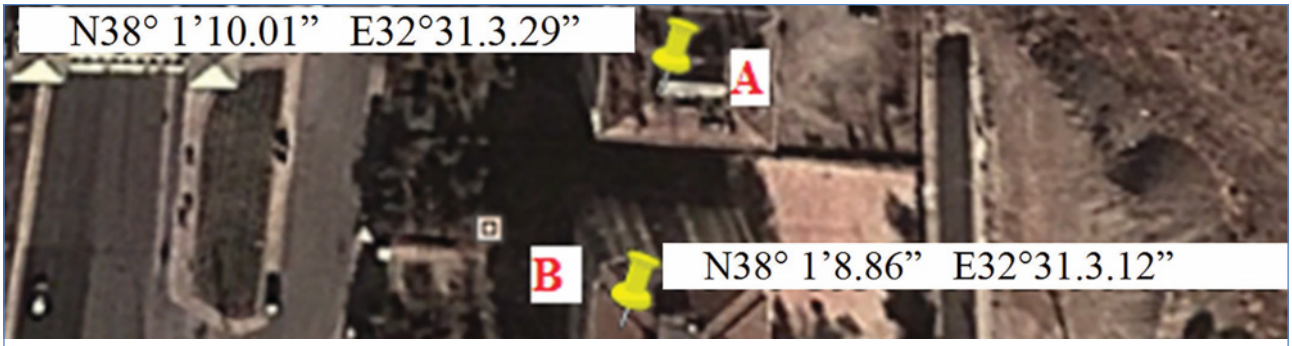

Figure 4: Coordinates of the measurement locations

weaker inside a car because of the car's metallic structure, so the mobile phone has to raise its output power to maximum to keep the connection going. This theoretically means that speaking with a mobile phone inside a car increases EM radiation exposure to nearby humans.

Other Use Cases

We used the instantaneous mode of our radiation meter in cases of calling, speaking and sending texts with the mobile phone. The coordinates for the measurement location are 38°1'50.11"K 32°30'.45.13"D; the actual measurements are shown in Table 3.

Additionally, we carried out measurements to compare 2G (conventional) and 3G (video calling) usage during speaking at two different location points, one of which in a direct line of sight to the base station. The recorded values using the maximum mode of the device are shown in Table 4.

Outdoor Measurements

Another set of measurements were made on a base station placed on the roof of a building – see Figures 4 and 5. The averaged EM radiation values are shown in Table 5. Results showed that, despite popular belief, EM radiation in buildings around the base station was higher than in the building under the base station.

We then checked EM radiation with respect to distances to the base station from our Selçuk University campus; see Table 6 and Figure 6.

We also found that more EM radiation was emitted during the first 4-5 seconds of calling until a connection is established, which decreases by a bit during speaking. Additionally, it was determined that EM radiation during speaking with a mobile phone was higher than when sending SMS. It should be also noted that EM radiation exposure time of sending SMS is a short duration of 1-2 seconds.

Rittal – The System.
Faster – better – everywhere.
Box smarter with Rittal
■ Superior quality
■ Extensive size range
■ Comprehensive product options
■ Instant availability
■ Competitive pricing
ENCLOSURES
POWER DISTRIBUTION
CLIMATE CONTRO

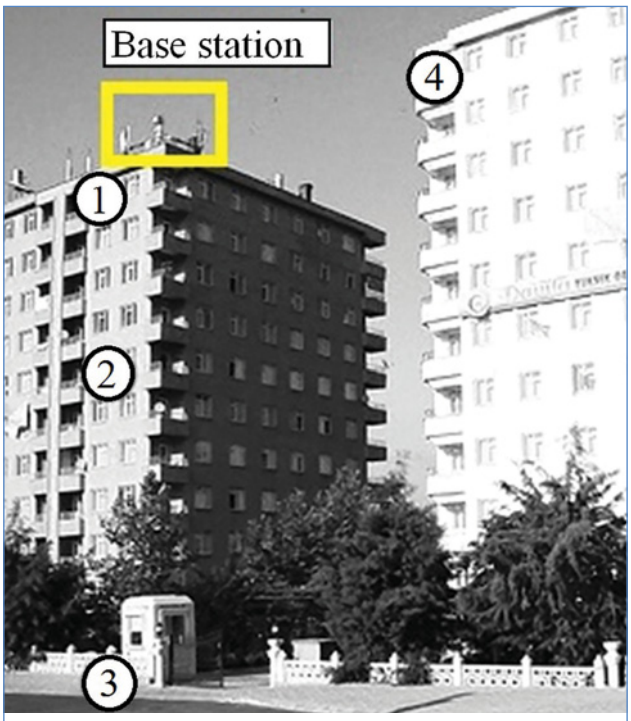

Figure 5: Measurement points

Another observation was that EM radiation levels during a video call using 3G are much higher than when using audio only.

Our study showed that the effect of location and distance to the base station matter when it comes to EM radiation levels: EM radiation in flats of a building with a base station on its roof was lower than in the flats of buildings around the base station.

When it comes to the effect of distance, it was observed that up to 80m the EM radiation level was increased and after this distance it starts to decrease as the distance to the base station increases. ●

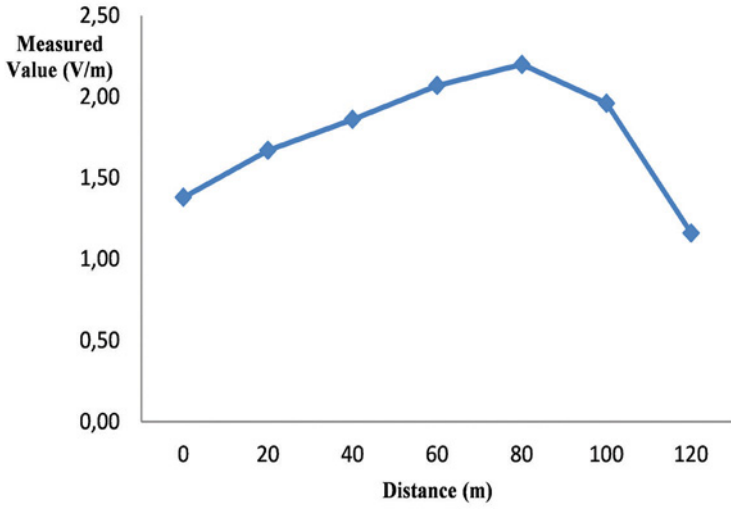

Figure 6: Measurement graph with respect to distance to the base station

REDUCING RF ABSORPTION FROM MOBILE PHONES

MOHAMMAD RASHED IQBAL FARUQUE FROM UNIVERSITI KEBANGSAAN IN MALAYSIA PRESENTS A NOVEL DOUBLE-NEGATIVE TRIANGLE METAMATERIALS STRUCTURE FOR REDUCING RADIATION EXPOSURE

The interaction of signals from handset antennas with the human body is of particular interest to the cellular communications community. The user's body, especially head and hands, influence the antenna's voltage standing-wave ratio (VSWR) and gain, as well as the radiation patterns. Furthermore, thermal effects, particularly when tissues are exposed to unlimited amounts of electromagnetic energy at certain frequencies, can be a serious health risk.

To address these risks, standardization bodies have set exposure limits relating to the human body's specific absorption rate (SAR). Simplified phone antennas, such as half-wavelength dipoles in free space or quarter-wavelength monopoles mounted on a metallic box, have been thoroughly investigated in the literature. These antennas are no longer in widespread use for cellular phones; however, for modelling purposes, it is reasonable to use a simple monopole or dipole antenna and, currently, planar inverted F-antennas (PIFAs) and helical antennas are two of the most commonly used.

Modern handset antennas are designed to support two or more frequency bands of various cellular networks. Consequently, a comprehensive study is required to determine which antenna offers better performance and is a lower health risk.

Solving The EM Challange

It has been shown that strategically placing a shielding material inside a cellular phone helps reduce SAR. This can be further improved by using a metamaterial in the design phase. Placing a perfect electric conductor (PEC) reflector over the phone's driver circuit of a folded loop type antenna was first proposed by Tay et al in 1998.

Metamaterials are engineered materials that demonstrate properties not naturally found in their constituent components. These artificially-structured composites have the potential to operate in critical voids in the electromagnetic spectrum where other material's responses are restricted, and enable the construction of novel devices. More recently, metamaterials displaying negative refractive index-a property not seen in nature have drawn considerable interest, emphasising their potential for various electromagnetic applications.

Important Parameters

There are two parameters important in metamaterials: electric permittivity and magnetic permeability, which determine the material's response to electromagnetic fields. The electric permittivity determines the electric field's distribution in the material, and magnetic permeability indicates the ability of the material to form a magnetic field within itself. Typically,

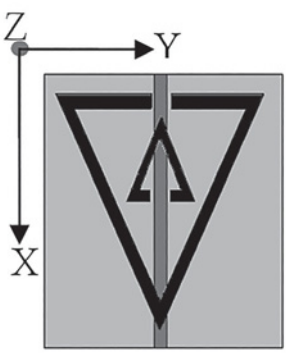

Figure 1a: TSRR structure

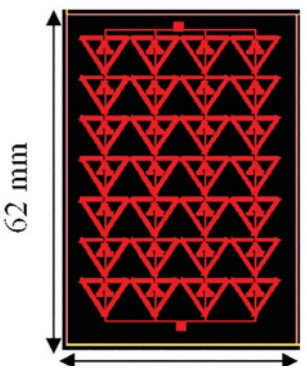

Figure 1b: Arrays of TSRRs used in our calculation

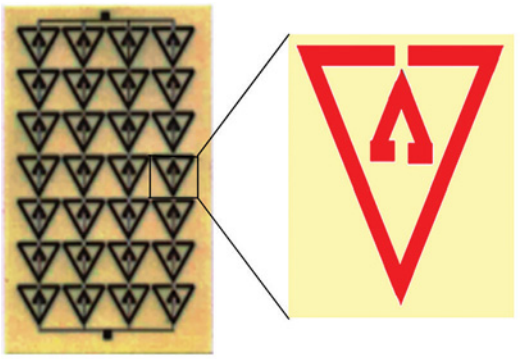

Figure 1c: Fabricated TSRR structure for SAR measurements

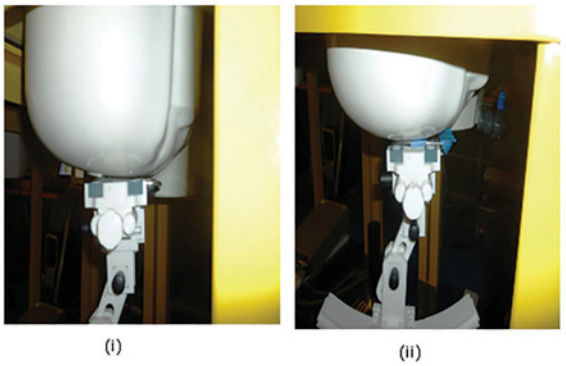

Figure 2a: Measurement of the SAR values at the cheek position (i) without metamaterial and (ii) with metamaterial

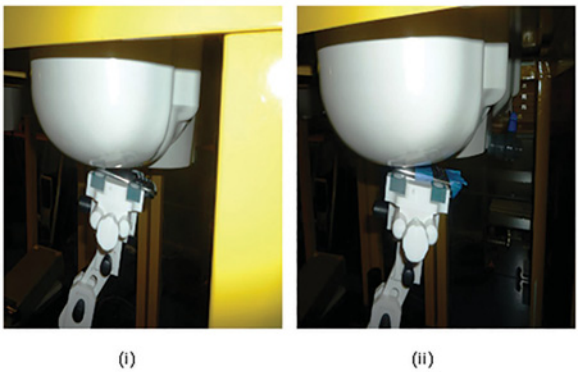

Figure 2b: Measurement of the SAR values at the tilt position (i) without metamaterial and (ii) with metamaterial

metamaterials consist of a copper structure on a substrate (circuit board), so they can easily be integrated into a mobile phone.

To study the SAR reduction of an antenna operated in the GSM 900 band, the effective medium parameter of meta-materials is set to be negative at 900MHz. Different positions, sizes and negative medium parameters of metamaterials for SAR reduction effectiveness are also analyzed.

Materials And Methods

In mobile phones, antennas are normally back-mounted and the metamaterial is placed on the front of the phone, just opposite the display, so that it shields the head.

In our study, we used a PIFA-based handset and a SAM phantom head (see Figure 2) provided by CST Microwave Studio (CST MWS). To accurately characterise the performance over a broad frequency range, dispersive models for all dielectrics were adopted. We used a helical PIFA for our simulations, operating at 900MHz (GSM).

Any SAR of the head is reduced by placing triangular-shaped metamaterials (TMMs) smaller than the operating wavelength. The structures are resonant due to their internal capacitance and inductance.

Our research helped us establish that TMMs can be used to reduce peak SAR using finite-difference time-domain (FDTD) analysis.

TMM arrays can be formed by arranging a pattern of triangular split ring resonators (TSRRs). The TSRRs' structure consists of two concentric triangles of conductive material. Both triangles have a gap, and each ring is placed opposite the gap of the other (see Figure 1a).

The TSRR arrays, 62mm × 38mm each, are shown in Figure 1b. These arrays were divided into four columns and seven rows. Figure 1c shows the fabricated TSRRs used for SAR measurements.

To construct the TMMs for SAR reduction, TSRRs were used as resonators. They resonate at approximately half of the guided-wavelength of the resonant frequency.

There are two resonances from each TSSR: the resonance of the outer triangle is at a lower frequency.

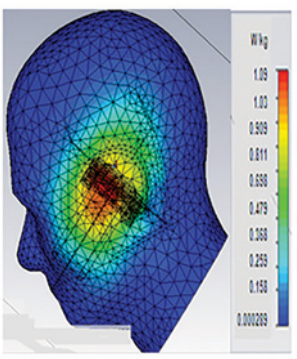

Figure 3a: Simulated SAR of the antenna with TMM array attached in tilted position

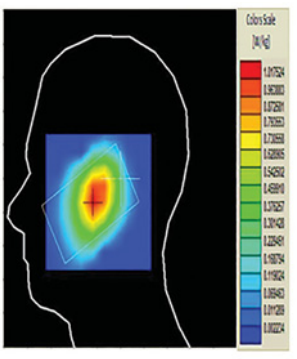

Figure 3b: Measured SAR of the antenna with TMM array attached in tilted position

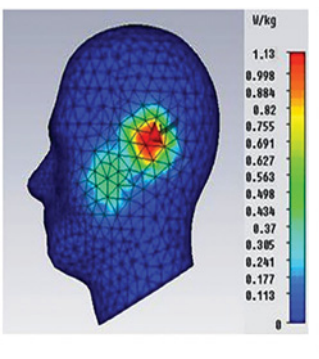

Figure 3c: Simulated SAR of the antenna with TMM array attached in cheek position

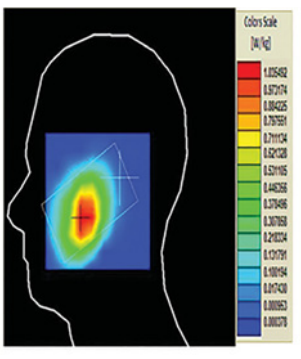

Figure 3d: Measured SAR of the antenna with TMM array attached in cheek position

	Value of SAR	
	SAR 1gm	SAR 10gm
Simulated	2.002	1.673
Measured	1.936	1.609

Table 1: SAR simulation and measurement results without TMMs (distance between head and phone d = 20 mm)

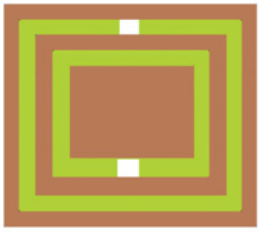	51.43+j99.68	514.6	211.95	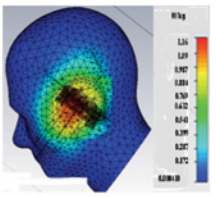	1.1623 / 0.737
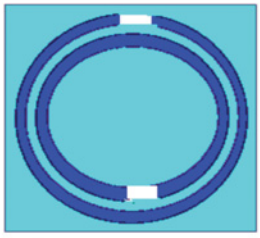	52.28+j99.98	528.7	224.63	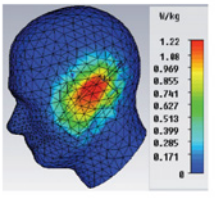	1.2271 / 0.781
	51.04+j98.94	512.7	206.83	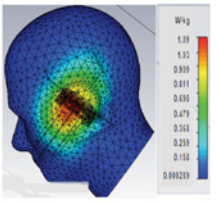	1.0963 / 0.676

Table 2: Comparisons of the effects of different metamaterial designs on SAR reduction (PR = 0.5W for 900MHz)

Figures 2a and b show the test setup for the cheek position and tilted position measurements to determine the SAR values. Figures 2a (i) and (ii) show the head position and setup without and with the TMM attachment. Figure 2b (i) and Figure 2 (ii) likewise show the 15° tilt position without and with TMM attachment.

Figures 3a and b show the simulated and measured SAR values obtained in tilted position for the TMMs and the antenna, which resulted in simulated and measured SAR 1gm values of 1.0963W/kg and 1.017W/kg, respectively. The simulated and measured SAR values differed by 7.23% for SAR 1gm value (where 1gm and 10gm are the sample volumes for tissue).

Conclusion

Based on the 3D FDTD method with lossy-Drude model, our study showed that using a metamaterial in the phone, SAR can be reduced to around 65%W/kg for a sample value of 10gm of tissue and around 51%W/kg for 1gm (see Table 1).

Considering different type dielectric metamaterials and varying their ε and μ values to divert the electromagnetic energy from the user's head are also options for further studies, which seem promising for improving SAR reductions (see Table 2). ●

Electronics WORLD

Your essential electronics engineering magazine and technical how-to-guide

A subscription to Electronics World offers

- 12 monthly issues in digital format
- Regular topical supplements
- The Annual T&M Supplement
- Weekly email bulletin
- Comment and analysis from industry professionals
- Tips and tricks
- News and developments
- Product reviews
- Free invitations to our webinars

Electronics World provides technical features on the most important industry areas, including:

- Nano measurement
- Robotics, and much more...
- DSPs
- Power supplies
- Automotive
- Lighting USB design
- Power supplies
- Test and measurement
- Cables
- Signal processing
- Connectors
- Semi-conductors
- Digi
- Embedded
- Microwave
- RF
- Communica-tions

SUBSCRIBE TODAY FROM JUST £46 BY VISITING THE WEBSITE OR CALLING +44(0)1635 879 361

www.electronicsworld.co.uk/subscribe

Register for our free newsletter, please scan here

MANAGING RISK FOR MEDICAL DEVICES

Medical device testing

BY **JEAN-LOUIS EVANS**, MANAGING DIRECTOR OF THE GLOBAL PRODUCT TESTING AND CERTIFICATION ORGANISATION TÜV SÜD PRODUCT SERVICE

The Third Edition of the Medical Electrical Equipment Standard (EN 60601-1:2006) was the first of its kind to incorporate risk management in the design and production of devices. Traditionally, test standards have developed more slowly than medical technologies have, so this standard aims to reduce such disconnect, so that safety legislation keeps pace with both the rapid changes in technologies and their fast adoption.

Keeping Files

The previous edition of the standard was entirely test-based; however, the Third Edition requires recording a detailed risk management file (RMF), with many of the compliance tests referencing that RMF.

Clause 4.2.2 of the Standard states: "A risk management process complying with ISO 14971 shall be performed". This means that, to meet the requirements of the standard, a manufacturer must have a process in place that complies with ISO 14971 *'Application of Risk Management to Medical Devices'*.

The Third Edition also has over 150 direct links to risk management and requires that the detailed RMF is updated as a "live" document, in order to match any changes deriving from design and/or manufacturing processes, or from new risks not evaluated before.

The RMF allows the required testing process to be modified depending on how the device must comply with some aspects of the standard. A good example of this is some medical equipment having to be robust enough for use in extreme environmental conditions on the battlefield, for example.

Whereas in the past there was a simple 'pass' or 'fail' against test criteria; now, if a device does not meet some of the standard's test criteria (often because it is a new technology not yet covered by the standard), manufacturers can mitigate that risk within the RMF. They do this by providing a rationale of the associated risk and why the product is still safe to use.

In theory, if manufacturers can show 'equivalent safety', they can substitute or deviate from test-based requirements by using the RMF. Equivalent safety is described in clause 4.5, which allows the manufacturer to use an alternative means of managing any risk addressed by the standard, as long as the residual risk (estimated as part of the risk management process) can be demonstrated to be equal or less than the residual risk that results from applying the requirements of the standard. However, this will not apply in all cases, as there are many tests in the standard that must have either a 'pass' or 'fail' and do not allow for equivalent safety to be shown or rationalised through the RMF.

There are in the region of 300 pass/fail verdicts, some of which are test-based and others risk-management-based. While a manufacturer may be able to prove an excellent risk rationale or 'equivalent safety', parts of the standard remain compulsory, as some elements would be almost impossible to justify, for example electrical leakage currents.

While the risk management process allows designers more flexibility, the RMF should not be viewed as a "catch all" that can be used to ignore test failures. You must still demonstrate that the risk assessment takes into account applicable regulations and standards, stakeholder concerns and state-of-the-art processes, and that acceptable risks are rationally based and measurable.

Continual Process

The risk management process includes a whole raft of considerations, including built-in safety, usability, installation, service, the expected use environment, what the equipment will be connected to and any unforeseen misuses. This actually strengthens the process since it is very difficult to consider all possible elements relevant to a specific piece of equipment in a traditional standard-based approach.

The risk management process must be used throughout the design process and product realisation, to determine whether or not a particular requirement is applicable, whether an alternative requirement can be substituted and if it can be satisfied with alternative test criteria or testing procedures. It is essential that any new product risk is first assessed and then any standard-compliance tests completed. This means thinking about the RMF at the beginning of product development and each subsequent stage.

But, how to assess risk?

Risk is a combination of probability of occurrence of harm and severity of that harm. Typically, a number is worked out for each and then multiplied to reveal the risk level. However, it is important to remember that this combination does not necessarily mean 'multiplication', as multiplying the numbers is not always reliable and a certain amount of common sense should also be used. It is therefore an important part of the risk management process not to just accept the final risk level, but review its likelihood and mitigate for it, if necessary.

For existing products, historical user data can be used as part of the risk management process, such as failures and accident rates. Also, look at customer complaints and warranty returns. If it is a new product with similar ones already on the market, it is also possible to benchmark against those and use their data.

> While a manufacturer may be able to prove an excellent risk rationale or 'equivalent safety', parts of the standard remain compulsory as some elements would be almost impossible to justify, for example electrical leakage currents

Misuse And Abuse

For the first time the Third Edition introduced the term 'essential performance', expanding the scope beyond basic safety requirements to ensure that a product performs as the end-user would expect. This also includes possible misuse within the RMF and ensuring that recommendations relating to it are included within the user manual. While there is no definite answer on how far a manufacturer has to apply this, the RMF is proof that misuse has been considered as far as practicable and mitigated against any possible risks to the best of abilities.

The Medical Devices Directive and the CB Scheme state that the risk management process must be verified by an auditor and part of this process will be to review the RMF. It is also logical that any certifying organisation will want to assess the manufacturer's risk management process as part of the certification process; no reputable certifier would just accept the manufacturer's file without a proper assessment.

Future Safety

Risk management should be the driver to make a medical device safe, not an excuse for designers and manufacturers to prove that they considered a risk, but didn't do anything about it. The RMF is actually a useful tool that helps reduce risks at all stages of product development and provides a genuine contribution to the product development process in order to improve a medical device. From product concept to end of lifetime, the risk management chain must be considered.

Medical operation

CONTROLLER SAVES SPACE WITH EVEN SMALLER FOOTPRINT

A new programmable DIN-rail mounted controller (PLC) from WAGO has a smaller footprint than its predecessors whilst providing enhanced functionality for seamless process automation. Available in three variants, the smallest of which is just 50mm wide, the PFC100 offers a compact and attractively priced control solution for a wide range of industrial applications.

The controller is designed exclusively for e!COCKPIT, WAGO's new intuitive engineering software suite, greatly simplifying the installation process and enabling systems to be brought online faster. Based on the Linux real-time operating system, the controller's Cortex A8 600MHz processor makes it suitable for highly complex algorithms and applications. The PFC100 combines comprehensive computing power and functionality of WAGO's feature-rich PFC family of controllers with a smaller footprint that can save considerable control-panel space.

PFC100 compact ECO version (750-8100) is scalable and extremely cost-effective.

http://global.wago.com/uk

TÜV SÜD LAUNCHES NEW ENVIRONMENTAL TESTING FACILITY

TÜV SÜD Product Service launched its new fast rate of change facility to help aerospace equipment manufacturers meet the RTCA DO-160requirements for environmental testing of electronic, electrical and mechanical systems in avionics.

The newly-upgraded TÜV SÜD facility includes a second fast rate of change test chamber that will increase capacity to minimise test waiting time and help manufacturers decrease time to market for new equipment. It will also cover a wider range of temperature fluctuations, in order to accurately replicate the rapid and extreme temperature variations experienced during flight, from -70°C to over 160°C, with temperature change rates up to 10°C per minute.

The facility complements a comprehensive selection of environmental test (climatic, vibration, etc) and EMC tests (lightning, power, etc) to deliver aerospace manufacturers the full range of avionics testing in a single location.

www.tuv-sud.co.uk

CONGATEC PRESENTS FIRST QSEVEN COMPUTER MODULES

Embedded computer systems maker congatec has extended its product portfolio for the most popular Qseven standard with Computer-on-Modules in the 40mm x 70mm sub-credit-card µQseven format.

The first flagship module of this new generation mini form-factor is the conga-UMX6 with ARM Cortex A9-based Freescale i.MX 6 processors. It caters to applications in harsh environments, which require not only compact low-power designs, but also appealing multimedia and computing performance. Applications benefit from the new conga-UMX6 µQseven computer modules' ARM-consistent, long-term availability of 10+ years, high performance per watt with a typical power consumption of just 3.5W, plus extended temperature support of -40°C to +85°C.

The feature-set of the new application-ready congatec µQseven modules is perfectly tailored for traffic systems, in-vehicle systems, small size PLCs, parking ticket machines and any other embedded or IoT application.

www.congatec.com

BULGIN LAUNCHES NEW MINIATURE ANTI-VANDAL SWITCH RANGE

Bulgin has extended its popular range of anti-vandal products to include a 12mm miniature push-button variant. This is the smallest and most versatile of its kind, with multiple actuator options and a life expectancy guaranteed to 200,000 cycles. Compact and durable, it is ideal for applications where space is at a premium.

The IP65- and IK08-rated miniature anti-vandal range (IP67-rated switches available to order) is perfect for demanding environments where reliability is vital, with an operating temperature between -25°C and +55°C and shock resistance greater than 10g. Screw and pin terminal options with ratings up to 36V DC, 2A are available in a wide variety of actuator and body types, including: nickel-plated brass, stainless steel, zinc-aluminium and chrome-plated, domed, flush and raised actuator options in stainless steel or PBT, dot and ring LED illuminated variants and others.

www.bulgin.com

NEW HIGH-ACCURACY, HIGH-ISOLATION, DIFFERENTIAL CURRENT SENSOR ICS

Allegro MicroSystems Europe launched two new current sensor ICs that are economical and precise solutions for AC or DC current sensing. The new devices are ideal for industrial, commercial and communication systems that require very high voltage isolation.

Both the ACS724KMA (5V) and ACS725KMA (3.3V) are available in very small package, suitable for space-constrained applications, also saving on cost through reduced board area.

The differential sensing technology provides immunity to interfering common mode magnetic fields from adjacent current traces or motors. Typical applications include motor control, load detection and management, switched-mode power supplies and overcurrent fault protection.

Both devices consist of a precise, low-offset, linear Hall sensor circuit with a copper conduction path located near the surface of the die.

www.allegromicro.com

HIGH-PERFORMANCE UNCOOLED THERMAL CAMERA CORE

FLIR Systems announced Boson, its smallest, lightest and least power-consuming, high-performance uncooled thermal camera for OEMs. Sized between FLIR's Tau and Lepton camera cores, Boson is the first thermal camera core to incorporate a sophisticated, low-power multi-core vision processor based on the FLIR XIR expandable infrared video processing architecture.

Boson features a high-sensitivity 12-micron pixel pitch detector that provides high-resolution thermal imaging in a small, low power, lightweight, turnkey package. It also offers several levels of video processing with inputs, and processing for other sensors including visible CMOS imaging sensors, Global Positioning Systems (GPSs) and Inertial Measurement Units (IMUs). Additionally, FLIR XIR offers a suite of advanced image processing features including super resolution algorithms, sophisticated noise reduction filters, local area contrast enhancement and image blending.

www.flir.com

PROTEUS 8.3

ECAD to MCAD made easy

Data Exchange with STEP/IGES

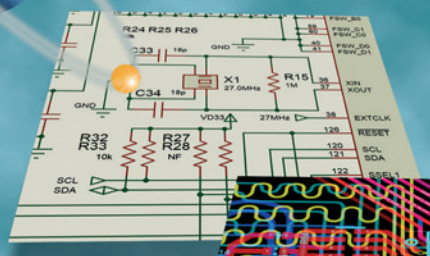

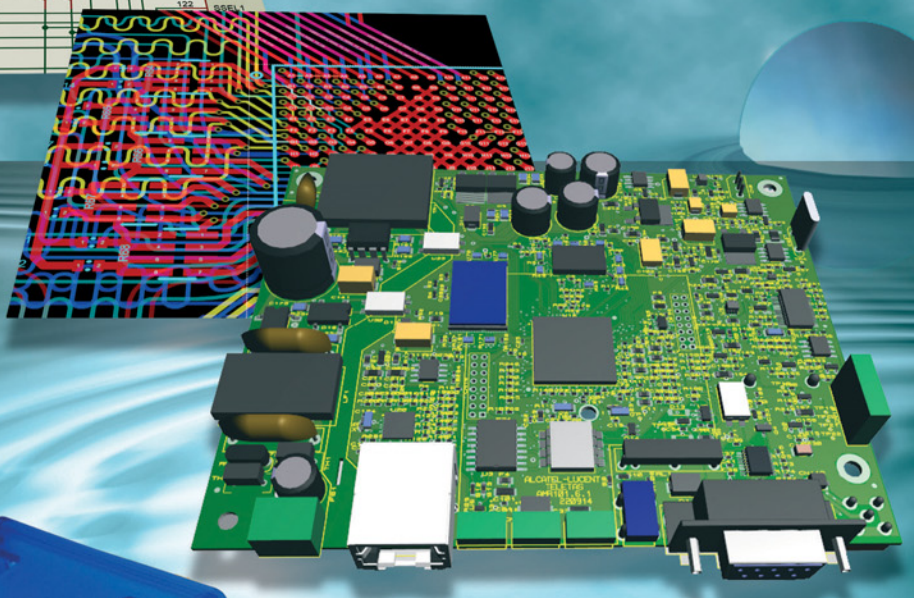

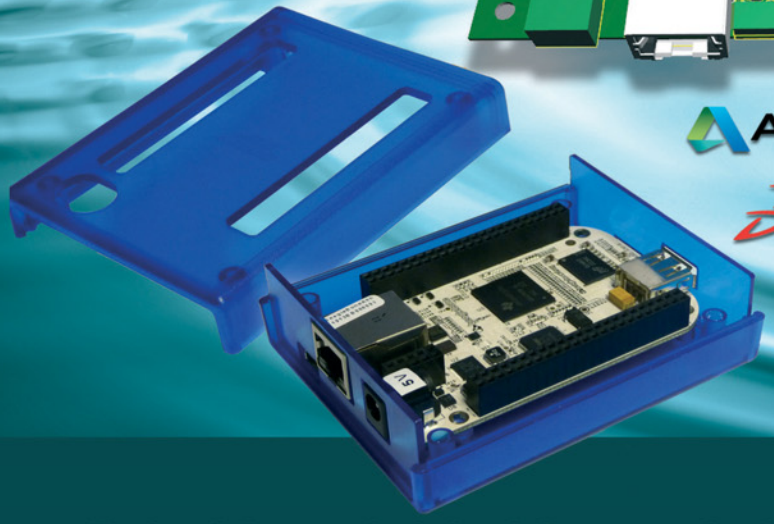

AUTODESK. PTC

SOLIDWORKS

The Proteus Design Suite now includes full support for data exchange with Mechanical CAD packages via the STEP/IGES file formats. This allows you to better visualise your design and helps quickly solve fixtures, fittings and casement problems.

Import 3D STEP/IGES models for your parts and visualise inside the Proteus Design Suite. Export your completed board to Solidworks or other MCAD software.

Visit www.labcenter.com

Tel:+44 01756753440 E-Mail info@labcenter.com

Labcenter Electronics Ltd, 21 Hardy Grange, BD23 5AJ

Labcenter Electronics www.labcenter.com

Authorised global distributor of the **NEWEST** electronic components.

mouser.co.uk/new

You can't design the future with the products from the past.

Design with the **NEWEST** PRODUCTS ahead of their time.

MOUSER ELECTRONICS

The Newest Products for Your Newest Designs®

Mouser and Mouser Electronics are registered trademarks of Mouser Electronics, Inc. Other products, logos, and company names mentioned herein, may be trademarks of their respective owners.